

Journal Pre-proofs

Design and synthesis of cyanamides as potent and selective N-acylethanolamine acid amidase inhibitors

Michael S. Malamas, Shrouq I. Farah, Lamani Manjunath, Dimitrios N. Pelekoudas, Nicholas Thomas Perry, Girija Rajarshi, Christina Yume Miyabe, Honrao Chandrashekhar, Jay West, Spiro Pavlopoulos, Alexandros Makriyannis

PII: S0968-0896(19)31419-1
DOI: <https://doi.org/10.1016/j.bmc.2019.115195>
Reference: BMC 115195

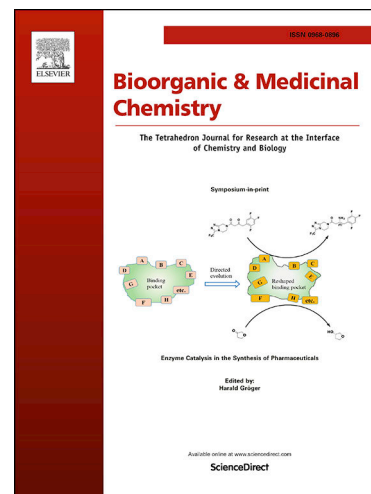
To appear in: *Bioorganic & Medicinal Chemistry*

Received Date: 21 August 2019
Revised Date: 29 October 2019
Accepted Date: 30 October 2019

Please cite this article as: M.S. Malamas, S.I. Farah, L. Manjunath, D.N. Pelekoudas, N. Thomas Perry, G. Rajarshi, C. Yume Miyabe, H. Chandrashekhar, J. West, S. Pavlopoulos, A. Makriyannis, Design and synthesis of cyanamides as potent and selective N-acylethanolamine acid amidase inhibitors, *Bioorganic & Medicinal Chemistry* (2019), doi: <https://doi.org/10.1016/j.bmc.2019.115195>

This is a PDF file of an article that has undergone enhancements after acceptance, such as the addition of a cover page and metadata, and formatting for readability, but it is not yet the definitive version of record. This version will undergo additional copyediting, typesetting and review before it is published in its final form, but we are providing this version to give early visibility of the article. Please note that, during the production process, errors may be discovered which could affect the content, and all legal disclaimers that apply to the journal pertain.

© 2019 Elsevier Ltd. All rights reserved.



Design and synthesis of cyanamides as potent and selective N-acylethanolamine acid amidase inhibitors

Michael S. Malamas ^{*1}, Shrouq I. Farah ¹, Lamani Manjunath ¹, Dimitrios N. Pelekoudas ¹, Nicholas Thomas Perry ¹, Girija Rajarshi ¹, Christina Yume Miyabe ¹, Honrao Chandrashekhar ¹, Jay West ¹, Spiro Pavlopoulos ¹ and Alexandros Makriyannis ^{*1}.

¹Center for Drug Discovery and Departments of Chemistry and Chemical Biology and Pharmaceutical Sciences, Northeastern University, Boston, Massachusetts 02115, United States

Abstract

N-acylethanolamine acid amidase (NAAA) inhibition represents an exciting novel approach to treat inflammation and pain. NAAA is a cysteine amidase which preferentially hydrolyzes the endogenous biolipids palmitoylethanolamide (PEA) and oleoylethanolamide (OEA). PEA is an endogenous agonist of the nuclear peroxisome proliferator-activated receptor- α (PPAR- α), which is a key regulator of inflammation and pain. Thus, blocking the degradation of PEA with NAAA inhibitors results in augmentation of the PEA/PPAR- α signaling pathway and regulation of inflammatory and pain processes. We have prepared a new series of NAAA inhibitors exploring the azetidine-nitrile (cyanamide) pharmacophore that led to the discovery of highly potent and selective compounds. Key analogs demonstrated single-digit nanomolar potency for hNAAA and showed >100-fold selectivity against serine hydrolases FAAH, MGL and ABHD6, and cysteine protease cathepsin K. Additionally, we have identified potent and selective dual NAAA-FAAH inhibitors to investigate a potential synergism between two distinct anti-inflammatory molecular pathways, the PEA/PPAR- α anti-inflammatory signaling pathway¹⁻⁴, and the cannabinoid receptors CB1 and CB2 pathways which are known for their antiinflammatory and antinociceptive properties⁵⁻⁸. Our ligand design strategy followed a traditional structure-activity relationship (SAR) approach and was supported by molecular modeling studies of reported X-ray structures of hNAAA. Several inhibitors were evaluated in stability assays and demonstrated very good plasma stability ($t_{1/2}$ > 2 hours; human and rodents). The disclosed cyanamides represent promising new pharmacological tools to investigate the potential role of NAAA inhibitors and dual NAAA-FAAH inhibitors as therapeutic agents for the treatment of inflammation and pain.

Keywords: N-acylethanolamine acid amidase (NAAA), N-palmitoylethanolamide (PEA), monoacylglycerol lipase (MGL), fatty acid amide hydrolase (FAAH), nuclear peroxisome proliferator-activated receptor- α (PPAR- α), CB1, CB2 cannabinoid receptors, anandamide (AEA), inflammation, antinociception.

* Corresponding author. Michael S. Malamas; E-mail address: m.malamas@northeastern.edu.

1. Introduction

Notwithstanding the major medical advancements over the past 50-years to treat inflammation and pain, still there is a great need for safer medications. The classic anti-inflammatory drugs, such as Nonsteroidal Anti-inflammatory Drugs (NSAIDs) are the most common used medications for the management of inflammation and pain, however their prolonged use is associated with severe side-effects, such as gastrointestinal ulcerations, bleeding, renal toxicity and cardiovascular injury. In order to minimize these undesirable side-effects, new pharmaceutical approaches were undertaken with drug delivery systems to achieve high drug concentrations at the site of inflammatory stimuli with minimal exposure to normal tissues⁹. While these drugs provided only limited success for the treatment of inflammatory conditions, as an alternate approach, one can envision the development of new therapeutic approaches to target the endogenous environment at the site of inflammatory stimuli. Along these lines, a family of endogenous bioactive lipids the N-acylethanolamines (NAEs) is considered to be implicated in the regulation of inflammation and pain¹⁰⁻¹². NAEs are not stored in cells, but rather synthesized “on-demand” upon inflammatory stimuli in most mammalian cells¹³. They are produced from membrane phospholipids by the sequential actions of N-acyltransferase to generate N-acyl phosphatidylethanolamines and phospholipase D (NAPE-PLD)¹⁴. Two endogenous N-acylethanolamines anandamide (AEA) and palmitoylethanolamide (PEA) are well-known to exhibit anti-inflammatory^{10, 11, 15} and analgesic¹⁶⁻¹⁸ properties. AEA suppresses inflammatory processes through stimulation of the cannabinoid receptors CB1 and CB2⁶, while PEA exerts its anti-inflammatory effects through interaction with the nuclear peroxisome proliferator-activated receptor- α (PPAR α)¹⁴. The physiological actions of these lipid messengers are terminated by two known intracellular lipid amidases fatty acid amide hydrolase (FAAH)¹⁹ and N-acylethanolamine acid amidase (NAAA)^{20, 21}, respectively. Pharmacological

inhibition of FAAH and NAAA augments the endogenous NAEs levels in rodent models promoting anti-inflammatory and analgesic effects^{10, 11, 15-18} without any cardiovascular effects and gastrointestinal hemorrhaging as frequently seen with cyclo-oxygenase-2 (COX-2) inhibitors²²⁻²⁴, further supporting their clinical development as an alternative therapeutic strategy against inflammatory diseases.

1.2. Role of NAAA inhibition in inflammation. NAAA is a lysosomal cysteine protease highly expressed in macrophages and peripheral tissues, including lungs and spleen⁹ and plays a central role in the deactivation of biolipid PEA. NAAA is activated by autoproteolysis at acidic pH ~ 4.5 conditions generating a catalytically competent subunit of the enzyme bearing a cysteine (Cys131 in mice, Cys126 in humans) as the nucleophilic residue responsible for the hydrolysis of PEA²⁵. PEA is an endogenous biolipid produced on-demand by most mammalian cells¹³ and a growing body of evidence links PEA to the regulation of inflammatory and pain processes. PEA reduces peripheral inflammation^{10, 26} and mast cell degranulation²⁷ and exerts neuroprotective²⁸ and antinociceptive effects¹⁶ in rats and mice. Local and systemic administration of PEA alleviated pain behaviors elicited by chemical irritants and was effective even when administered after induction of acute inflammation^{11, 17, 29}. In recent studies, NAAA inhibition increased the PEA levels at the site of inflammation in ulcerative colitis preclinical models and alleviated most of the symptoms of colitis, while significantly downregulated inflammatory cytokines levels at the gastrointestinal tract and peripheral tissues³⁰. Furthermore, other recent publications have reinforced the use of NAAA inhibitors for the treatment of chronic inflammatory disorders¹⁻⁴. Notwithstanding the encouraging pharmacological benefits of NAAA inhibitors in various inflammatory conditions, only a limited number of NAAA inhibitors with rather sub-optimal druggability profiles have been discovered to date.⁴

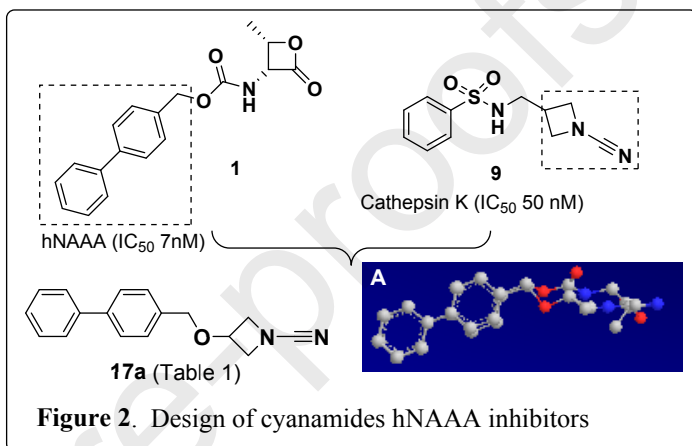
1.3. Endogenous PPAR- α activation in inflammation. The molecular thrust of PEA's anti-inflammatory effect is dependent on the activation of nuclear receptor peroxisome proliferator-activated receptor- α (PPAR- α), which is ubiquitously expressed in the brain, lung, liver, and intestinal mucosa of the small intestine and colon^{15, 31}. Thus, modulating the PEA/PPAR- α anti-inflammatory signaling pathway with NAAA inhibitors at the localized inflamed-tissue environment offers the opportunity to intervene locally with drugs and avoid broad receptor

them unfavorable as potential therapeutic candidates. Therefore, new generations of druggable NAAA inhibitors are needed to delineate the role of NAAA inhibition in inflammatory and pain processes.

2. Chemistry

2.1 Cyanamides hNAAA inhibitors. In

the design of a new series of NAAA inhibitors, we have merged two key structural pharmacophoric features comprised of the biphenyl tail of the known NAAA inhibitor **1**⁴⁰ (Fig. 1) and the azetidione-nitrile (cyanamide) pharmacophore of cathepsin K inhibitor **9**⁴⁵ (Fig. 2). In the design of this new

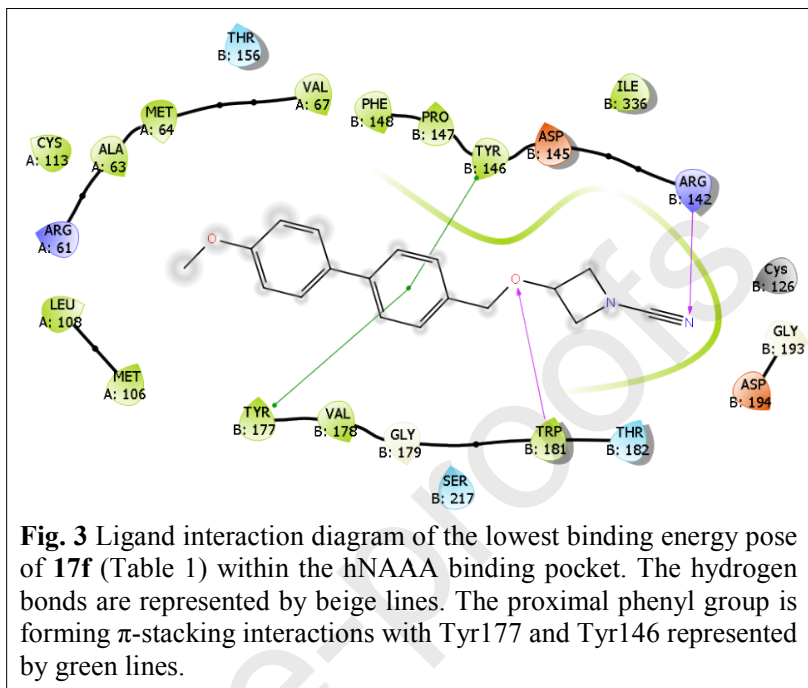


class of NAAA inhibitors, we have considered that both NAAA and cathepsin K are accountable for similar catalytic processes, considering that both belong to the N-terminal nucleophile (Ntn) lysosomal family of enzymes with comparable catalytic sites⁴⁶.

Further, cathepsin K drugs have been pursued as potential therapeutics for the treatment of osteoporosis.⁴⁵ Also, the NSAID agent diacerein used to treat osteoarthritis (OA)⁴⁷, was identified as a NAAA inhibitor⁴⁸. Also NAAA inhibitor **5** (Fig. 1; F215) was found to be a therapeutic agent for OA⁴⁹, indicative that NAAA may play a role in the pathogenesis of degenerative joint disease. Our primary objective in this study was to merge the two pharmacophoric features of compounds **1** and **9** (shown dashed-lines in Fig. 2) in an attempt to eliminate the high non-specific reactivity of the β -lactone of **1**, which showed high potency for NAAA with an IC_{50} value of 7 nM, but poor plasma stability ($t_{1/2} < 1$ min). At this stage of ligand design, we made the assumption that both NAAA inhibitor **1** and hybrid inhibitor **17a** (Fig. 2, Table 1) are active site inhibitors for NAAA. Conformational analysis of **1** and **17a** resulted in a good overlap of these two molecules (Cartoon A, Fig. 2). Armed with this information, we have prepared hybrid **17a** (synthesized according to scheme 1), which showed high potency for hNAAA using a fluorometric assay with an IC_{50} value of 2.8 nM after 90-minute pre-incubation period. At a shorter pre-incubation period (15 min), **17a**

had an IC_{50} value of about 17 nM, indicative of its irreversible or slow reversible (slow K_{off} rate) binding mode with the enzyme.

To better assess the potency of **17a**, we used a second order rate constant derived from the ratio of k_{inact}/K_I which has been suggested as the appropriate way to assess the potency of irreversible inhibitors. Unlike IC_{50} values, k_{inact}/K_I determinations are independent of pre-incubation times and therefore are a better measure of potency for assessing



irreversible inhibitors. Compound **17a** was found to have a high k_{inact}/K_I value of $3.03 \times 10^6 \text{ M}^{-1} \text{ s}^{-1}$ (Table 1), indicative of its high potency and its irreversible or very slow reversible binding mode.

2.2 Computer-assisted drug design. We were delighted that during our structure-activity relationship (SAR) studies a cocrystal structure of hNAAA was disclosed⁵⁰ and allowed us to use structural insights of the NAAA binding pocket to design new analogs. Examination of the “precovalent” binding pose of an early-on synthesized inhibitor **17f** (Table 1) revealed that the binding pocket of hNAAA predominately consisted of hydrophobic residues

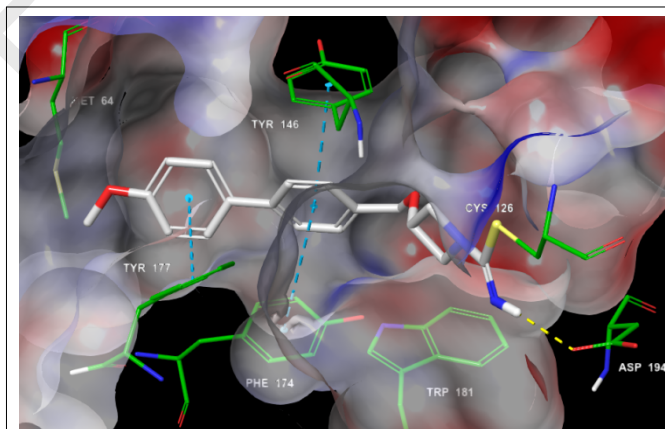


Fig. 4 Covalent docking of **17f** (Table 1) with hNAAA crystal structure with the leaving group no longer attached. A Connolly surface shown as electrostatic potential (red-white-blue) was used to represent the shape of the binding pocket. Only the key residues (green) and the ligand (white) are shown. All other atoms are colored by atom type. The ligand orients into the binding pocket making several π -stacking interactions shown in blue dashed lines. Hydrogen bonds are indicated by yellow dashed lines.

Tyr177, Trp181, Phe148, Tyr146, Met64 (Fig. 3; ligand interaction diagram of compound **17f** docked with hNAAA). The orientation of **17f** within the NAAA binding pocket closely resembled

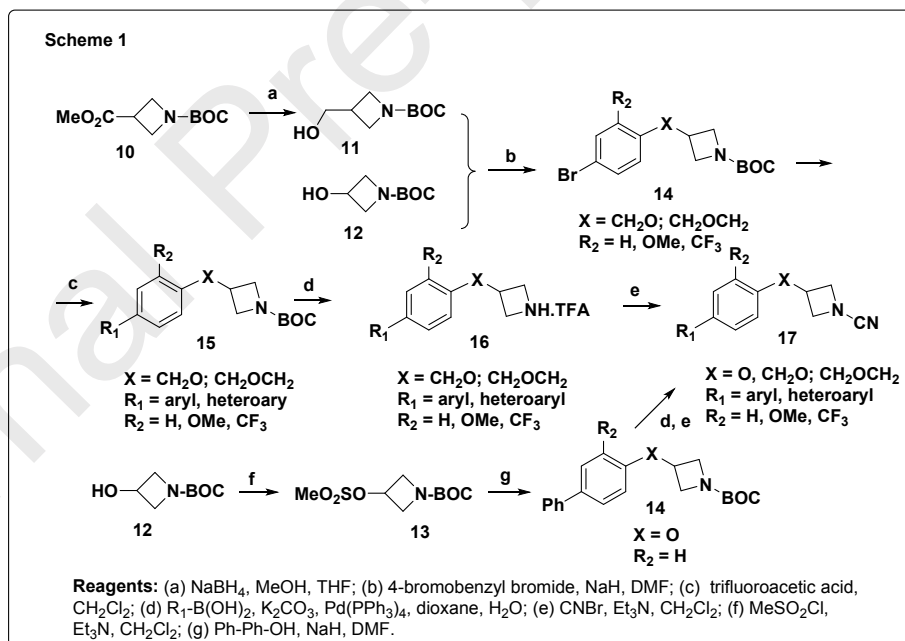
the endogenous substrate PEA (not shown), which carries a 15 carbon long alkyl tail occupying the hydrophobic binding pocket of NAAA. We have considered that the electrophilic cyanamide pharmacophore of compound **17f** upon interaction with the active site catalytic cysteine (Cys126) has triggered the formation of a covalent isothioureia adduct. Covalent docking of **17f** with hNAAA (Fig. 4) showed that the catalytic residue Cys126 of hNAAA was coupled with the electrophilic nitrile of the cyanamide group to form an isothioureia adduct. The rest of the ligand appeared to orient very similarly to that of the “precovalent” binding pose of the ligand within the binding pocket. The newly formed isothioureia adduct is time-dependently reversible⁴⁵ to regenerate the active enzyme. This interconversion process can be exploited by modifications of the ligand’s size (length and bulkiness) and generate analogs with different adduct residence time (τ). In contrast, fully irreversible adducts (suicidal inhibitors) have raised serious safety concerns in drug development because of the relationship between covalent drug binding and the potential of immunogenic-driven allergic reactions and idiosyncratic drug toxicity^{51, 52}.

2.3. New cyanamides

NAAA

inhibitors:

To further expand the scope and breadth of our initial findings and improve potency, selectivity and the ADME



properties of the molecule, we used molecular modeling strategies allowing us to construct “precovalent” NAAA-ligand poses using Glide/Prime to determine how the inhibitor fits into the binding site with the correct binding geometry. For molecules that geometrically fit into the NAAA binding pocket, we performed modeling studies to calculate the lowest free-binding energy of the ligand using the CovDock/Prime programs of the Schrodinger platform. During the optimization process, we have also employed cheminformatics

calculations (i.e. MW, ClogP, tPSA, LiPE) paying close attention to critical “drug-like” parameters to achieve stable and water-soluble molecules with good oral bioavailability. Examination of the reported hNAAA-inhibitor co-crystal⁵⁰ revealed that the NAAA active-site possesses high flexibility allowing several residues lining the binding cavity to attain adaptable conformations

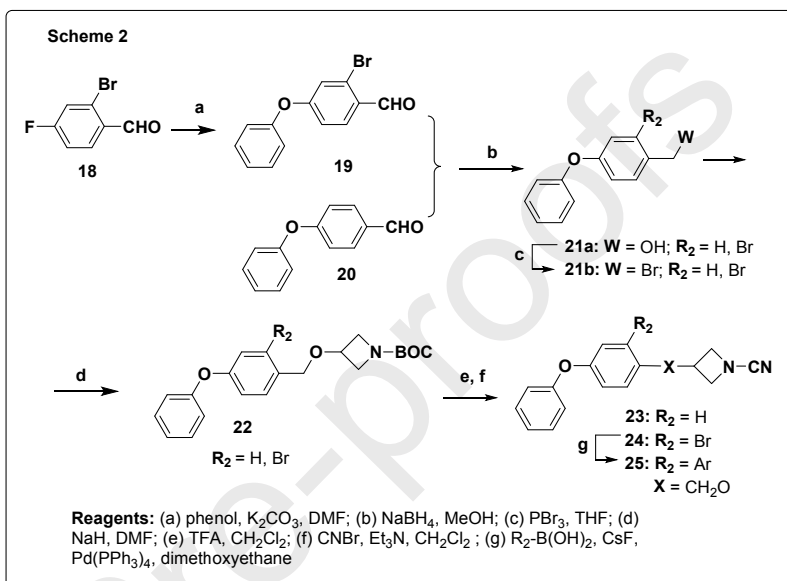
and accommodate structurally diverse ligands. Also, the computational studies revealed the presence of a hydrophobic cavity at the vicinity of the benzylic region (methoxy linker of compound **17f** Table 1), which was not occupied by the ligand (shown in

Fig. 4), representing an area for further exploration with new analogs (discussed below). We have routinely determined the lowest energy conformations of the ligands in the absence of protein and then compared it to the lowest energy conformers generated during “precovalent” docking to determine ligand adaptability within the binding pocket with minimal energy penalty for synthetic considerations. Structure-activity relationship studies have produced many compounds, and in this paper, we outline selected analogs in Tables 1 and 2.

2.4. Synthesis

The compounds needed to delineate the SAR for this study were prepared according to schemes 1-6.

2.4.1 Synthesis of alkoxy-linked analogs: In scheme 1, ester **10** was reduced with sodium borohydride in MeOH to afford alcohol **11**. Next, coupling either alcohol **11** or **12** with 1-bromo-4-(bromomethyl) benzene was accomplished by treatment with sodium hydride in N, N-dimethylformamide to produce **14** (X = CH₂O, CH₂OCH₂; R₂ = H). Palladium mediated cross-

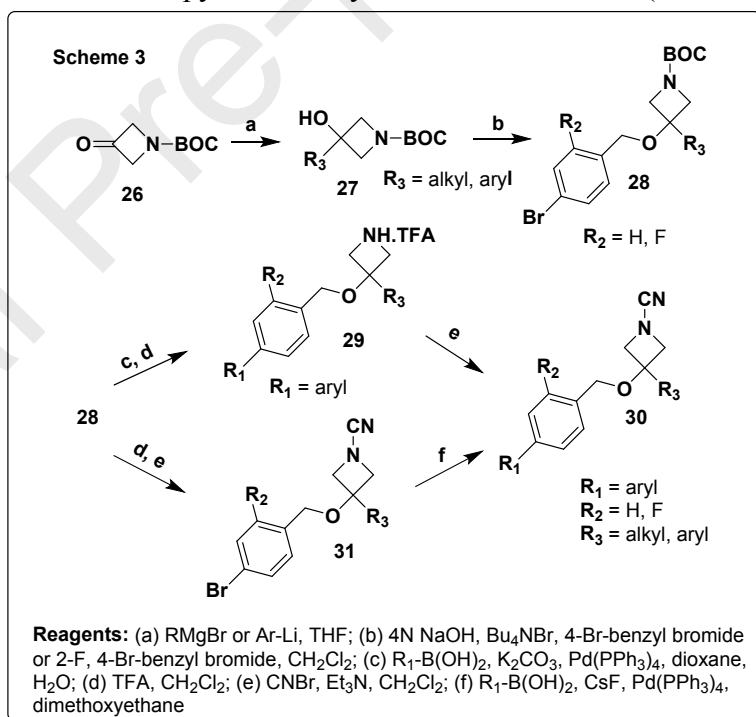


coupling reaction between the aryl-bromide **14** ($X = \text{CH}_2\text{O}$, CH_2OCH_2 ; $R_2 = \text{H}$) and an appropriate boronic acid in the presence of tetrakis (triphenylphosphine) palladium (0), K_2CO_3 and dioxane/water generated the biaryl product **15** ($R_1 = \text{aryl}$, heteroaryl). Unmasking the azetidine nitrogen of **15** with trifluoroacetic acid in dichloromethane afforded amine **16**, which upon treatment with cyanogen bromide and triethylamine in dichloromethane produced cyanamide **17** ($R_1 = \text{aryl}$, heteroaryl; $X = \text{CH}_2\text{O}$, CH_2OCH_2 ; $R_2 = \text{H}$).

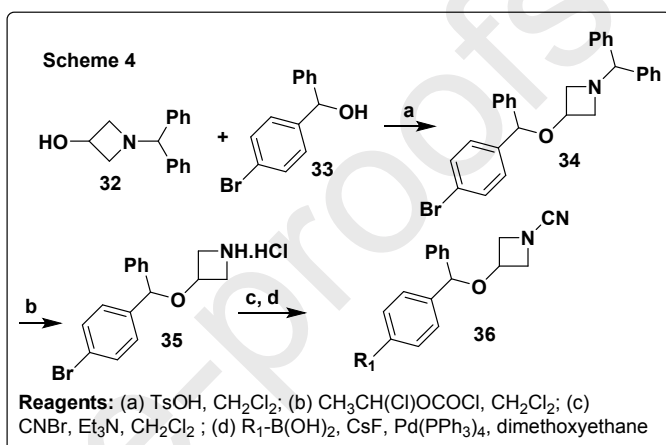
2.4.2 Synthesis of oxygen-linked analogs: In scheme 1, azetidin-3-ol **12** was treated with methanesulfonyl chloride and triethylamine to afford methane sulfonate **13**, which upon coupling with [1,1'-biphenyl]-4-ol in the presence of sodium hydride produced azetidine **14** ($X = \text{O}$; $R_2 = \text{H}$). Azetidine **14** was converted to the final cyanamide **17** ($X = \text{O}$; $R_2 = \text{H}$) as described above.

2.4.3 Synthesis of pyrrolidine-cyanamides: The pyrrolidine-cyanamides **42** and **43** (Table 1) were similarly prepared to the methods described for the synthesis of the azetidine-cyanamide **17** in scheme 1 by substituting azetidin-3-ol **12** with commercially available chiral (S)- and (R)-pyrrolidin-3-ols.

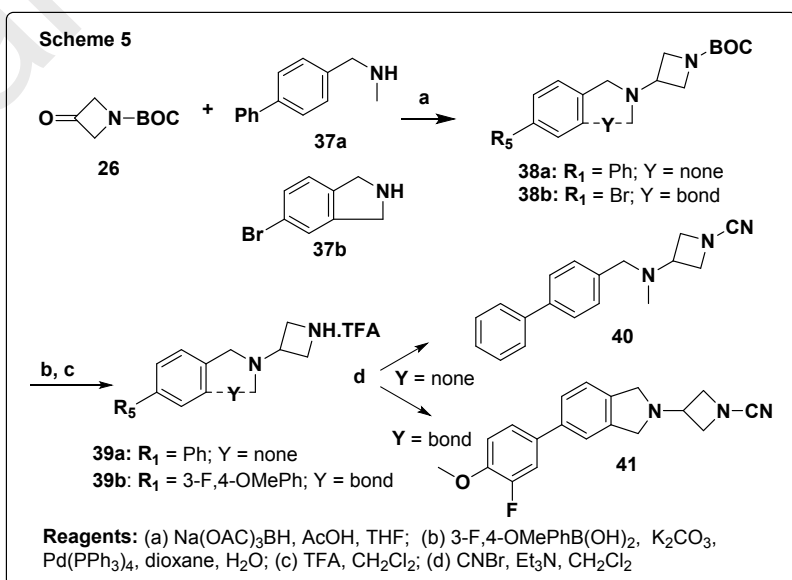
2.4.4 Synthesis of phenoxy-cyanamides: In scheme 2, the phenoxy-cyanamides **23-25** ($R_2 = \text{H}$, Br, aryl, $X = \text{CH}_2\text{O}$) were prepared as followed. Coupling of benzaldehyde **18** with phenol in the presence K_2CO_3 , in N, N-dimethylformamide afforded product **19**. Next, reduction of either aldehyde **19** or **20** (commercially available) with sodium borohydride gave benzylic alcohols **21a** ($R_2 = \text{H}$, Br), which were treated with phosphorus tribromide in tetrahydrofuran to afford benzyl bromides **21b** ($R_2 = \text{H}$, Br). Intermediates **21b** were converted to cyanamide **23-25** ($R_2 = \text{H}$, Br, aryl, $X = \text{CH}_2\text{O}$) similarly to the methods described in scheme 1.



2.4.5 Synthesis of 3,3-substituted azetidine cyanamides: In scheme 3, cyanamide **30** was prepared by two synthetic routes. (a) Treatment of 3-oxoazetidine **26** with alkyl- or aryl-Grignard or lithium reagents to produced alcohol **27** (R_3 = alky, aryl). Coupling of alcohol **27** under base-transfer conditions (sodium hydroxide, tetrabutylammonium bromide) with an aralkyl halide afforded azetidine **28** (R = aryl, heteroaryl; R_2 = H, F; R_3 = alky, aryl). Intermediate **28** was converted to azetidine **30** (steps c to e) similarly to the methods described in scheme 1. In an alternate route (b), the N-BOC intermediate **28** was first converted to cyanamide **31** (steps d and e) and then by application of the Suzuki coupling protocol (step f) afforded **30**, as described in scheme 2.



2.4.6 Synthesis of benzhydryl cyanamides: In scheme 4, the benzhydryl-cyanamide **36** was prepared by coupling of 1-benzhydrylazetidin-3-ol **32** with diphenyl-methanol **33** under acidic conditions (i.e. p-toluenesulfonic acid) to produce azetidine **34**. Unmasking the azetidine with 1-chloroethyl chloroformate, followed by treatment with BrCN/ Et_3N and the Suzuki arylation afforded benzhydryl-cyanamide **36** (R_1 = aryl, heteroaryl), as described in scheme 2.



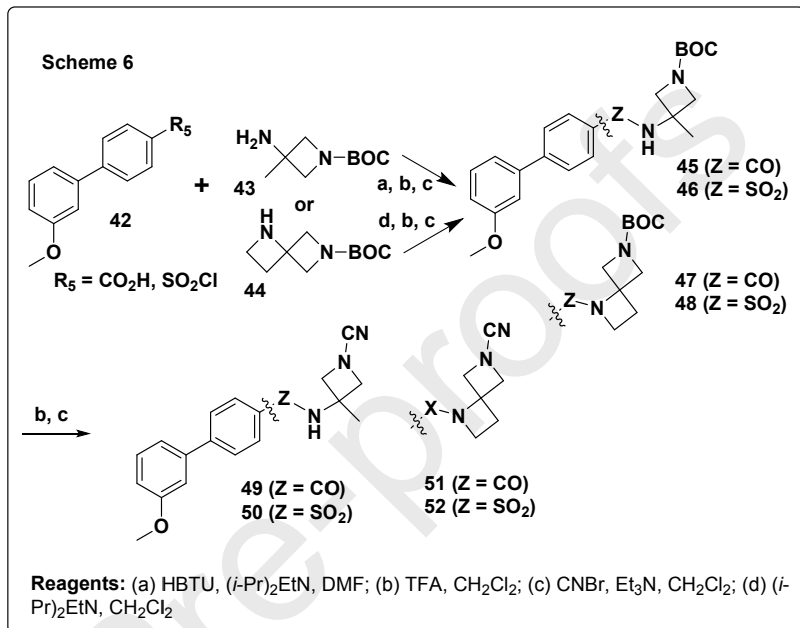
2.4.7. Synthesis of nitrogen-linked cyanamides: In scheme 5, the amino-cyanamide **40** and

the isoindoline-cyanamide **41** were prepared as followed. Reductive amination of 3-oxoazetidine **26** with either amine **37a** or **37b** using sodium triacetoxy borohydride under acidic conditions (i.e.

AcOH) produced azetidine **38a** ($R_1 = \text{Ph}$; $Y = \text{none}$) and **38b** ($R_1 = \text{Ph}$; $Y = \text{bond}$), respectively, which were converted to amino-cyanamides **40** and **41** according to the methods described in scheme 1.

2.4.8 Synthesis of amide- and sulfonamide-linked

cyanamides: In scheme 6, cyanamides **49-52** were prepared as followed. Benzoic acid **42** ($R_5 = \text{CO}_2\text{H}$) was coupled with amines **43** and **44** in the presence of HBTU and diisopropyl ethylamine to afford amides **45** and **47**, respectively. Sulfonamide **46** and **48** were prepared from benzene sulfonyl



chloride **42** ($R_5 = \text{SO}_2\text{Cl}$) and amines **43** and **44** in the presence of diisopropyl ethylamine. The BOC-protected intermediates **45-48** were converted to the final products **49-52** similarly to protocols described in scheme 1.

3. Results and discussion

All synthesized compounds were assessed in a fluorescence-based assay for NAAA inhibition with *N*-(4-methyl coumarin) palmitamide (PAMCA) as the substrate⁵³. Also, k_{inact}/K_I determinations were performed for a large set of compounds, however, the SAR development of this series of inhibitors was primarily based on IC_{50} determinations. Compounds that inhibited hNAAA with an IC_{50} value of < 30 nM were evaluated in selectivity counter screens. They were tested for their ability to inhibit human-recombinant FAAH (hFAAH)⁵⁴ and purified rat FAAH (rFAAH)⁵⁵ using the fluorogenic substrate arachidonoyl 7-amino-4-methylcoumarin amide (AAMCA)^{55, 56}. Following similar fluorometric procedures, all compounds were also tested against hydrolytic enzymes recombinant human monoacylglycerol lipase (hMGL)⁵⁷ and human alpha/beta-hydrolase domain containing 6 (hABHD6)⁵⁸ for selectivity. Also, selected inhibitors were evaluated in the

cathepsin K assay for selectivity against cysteine proteases⁴⁵. Furthermore, selected compounds were evaluated for their ability to bind to CB1 and CB2 receptors using rat brain⁵⁹ or HEK293 cell membranes expressing mouse CB2 (mCB2) or human CB2 (hCB2),⁶⁰⁻⁶² respectively, via competition-equilibrium binding using [³H]CP-55,940⁶¹⁻⁶³ to minimize/eliminate any potential cross-reactivity due to potential common pharmacophoric features.

A selection of compounds as described in the synthetic schemes (1-6) are shown in Tables 1 and

2. First, we studied the linker region of the biphenyl analog **17a** (Table 1).

Truncation of the methoxy-linker of **17a** by one carbon afforded phenoxy analog **17b**,

which was about 10-fold less potent for NAAA, while elongation by one carbon (analog **17c**) didn't

affect the ligand's potency. Replacement of the oxygen

with the N-Me group (compound **40**, Table 1)

resulted in about 7-fold loss

in potency. Next, we explored modifications at the distal phenyl group exemplified by entries **17d** to **17n** (Table 1). As we described above, induced-fit docking of **17f** with the hNAAA X-ray crystal structure (Fig. 5) suggested that there was unoccupied space at the binding pocket close to the

distal phenyl group of the ligand. We have introduced substitutions at the distal phenyl group to maximize ligand protein interactions. The *meta*-methoxy analog **17d** was found to be 3-fold more potent than the unsubstituted analog **17a**, by exhibiting sub-nanomolar potency for hNAAA. The longer bezylxyoxy-analog **17e**, the *para*-methoxy analog **17f** and the bulkier 2,3-disubstituted

methoxy analog **17g** also showed enhanced potency for NAAA when compared to **17a**. In contrast, the 2,6-disubstituted methoxy analog **17h** was about 70-fold less potent than **17g**. The 2,6-

dimethoxy substitution was not accommodated well at this region of the binding pocket, primarily

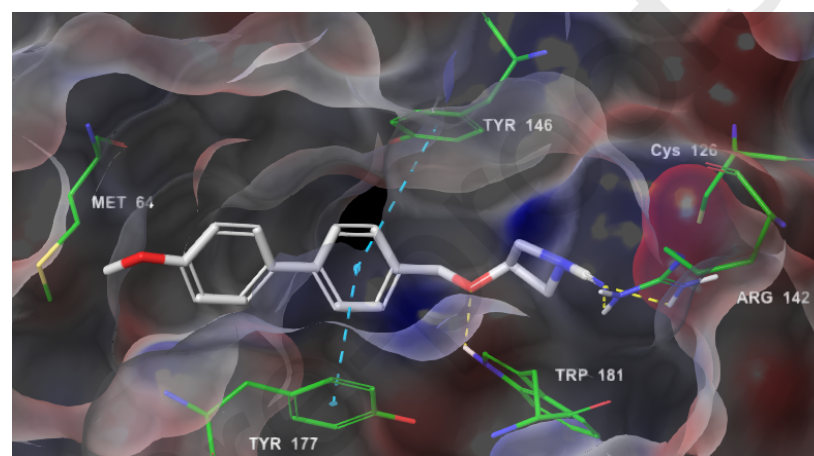


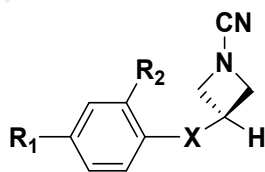
Fig. 5 Induced-fit docking of **17f** (Table 1) with hNAAA crystal structure. A Connolly surface shown as electrostatic potential (red-white-blue) was used to represent the shape of the binding pocket. Only the key residues (green) and the ligand (white) are shown. All other atoms are colored by atom type. The ligand orients into the binding pocket making several π -stacking interactions shown in blue dashed lines. Hydrogen bonds are indicated by yellow dashed lines

driven by conflict contacts between the ligand's distal phenyl group and nearby residues of the binding pocket wall (not shown). The 2,6-dimethoxy substitution pattern of the distal phenyl group has caused the ring to torque almost perpendicular to the proximal phenyl group of the molecule, thus positioning the ligand in an unfavorable orientation within the binding pocket and prevented it from making favorable van der Waals contacts with the protein and also hindered it from forming an efficient covalent adduct with the catalytic residue Cys126 of NAAA. The *para*-methyl analog **17i** was about 3-fold more potent than the analogous *para*-trifluoromethyl analog **17j**, while the smaller electronegative F-nucleus (analog **17k**) exhibited good sub-nanomolar potency. Replacement of the distal phenyl of **17f** with a pyridine moiety (entry **17l**) to improve the water solubility of the molecule resulted in about 40-fold loss of potency. Moving the 4-methoxy substituent of **17l** to the *ortho*-position (entry **17m**) it regained about 7-fold of its potency. The unsubstituted pyridine analog **17n** was about 4-fold less potent than the phenyl analog **17a**. We have postulated that the basic nitrogen of the pyridine's nucleus formed unfavorable electrostatic contacts with residues of the binding pocket causing a loss in potency.

Next, we have replaced the azetidine nucleus of **17a** with a pyrrolidine ring. Replacement of the azetidine nucleus with the five-membered pyrrolidine moiety (entry **42**) resulted in 10-fold loss of potency (**42** vs **17a**). The distomer analog **43** was even less potent (~100-fold) than **17a**.

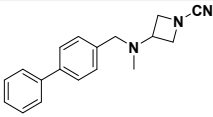
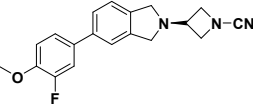
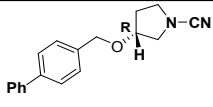
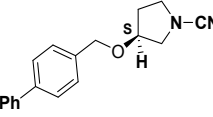
Several potent cyanamides (Table 1) with $IC_{50} < 30$ nM for hNAAA were evaluated in selectivity counter screens against serine hydrolases FAAH, MGL, ABHD6 and cysteine protease cathepsin K. All tested analogs exhibited weak to moderate selectivity (~5-20-fold; data not shown) against these hydrolases.

Table 1. Mono-substituted cyanamides hNAAA inhibitors



Compd	R ₁	R ₂	X	hNAAA	
				IC ₅₀ (nM) ± SD ^a	K _{inact} /K _i M ⁻¹ s ⁻¹
Biphenyl analogs					
17a	Ph	H	CH ₂ O	2.8±0.3	3.03x10 ⁶

17b	Ph	H	O	29±2	-
17c	Ph	H	CH ₂ OCH ₂	3.4±0.5	3.04 x10 ⁶
17d	3-OMePh	H	CH ₂ O	0.89±0.19	3.05 x10 ⁶
17e	3-benzyloxyPh	H	CH ₂ O	1.4	-
17f	4-OMePh	H	CH ₂ O	0.94±0.06	3.25 x10 ⁶
17g	2,3-di-OMePh	H	CH ₂ O	0.88±0.26	8.40 x10 ⁶
17h	2,6-di-OMePh	H	CH ₂ O	67.5	-
17i	4-Me-Ph	H	CH ₂ O	0.46±0.26	2.24 x10 ⁶
17j	4-CF ₃ -Ph	H	CH ₂ O	1.6±0.2	2.74 x10 ⁶
17k	4-F-Ph	H	CH ₂ O	0.68±0.25	2.09 x10 ⁶
17l	4-OMe- <i>m</i> -pyridyl	H	CH ₂ O	40±4	-
17m	2-OMe- <i>m</i> -pyridyl	H	CH ₂ O	5.8±0.4	-
17n	<i>m</i> -pyridyl	H	CH ₂ O	12±5	-
17o	3-OMePh	F	CH ₂ O	0.47±0.17	1.73 x10 ⁶
17p	3-OMePh	CF ₃	CH ₂ O	0.85±0.21	1.40 x10 ⁶
17q	3-OMePh	OMe	CH ₂ O	2.8±0.2	-
Benzyloxy analogs					
23	PhO	H	CH ₂ O	1.1±0.05	1.33 x10 ⁶
24	PhO	Br	CH ₂ O	1.03±0.05	-
25a	PhO	Ph	CH ₂ O	8.5±1	-
25b	PhO	2-OMe-Ph	CH ₂ O	23.7±2.2	-
25c	PhO	4-OMe-Ph	CH ₂ O	5.7±0.3	-
25d	PhO	4-CN-Ph	CH ₂ O	2.5±0.3	-
25e	PhO	2-CN-Ph	CH ₂ O	6.6±0.3	-
Benzhydryl analogs					
36a	3-OMePh	H	CH(Ph)O	11.6±0.5	-

36b	3,5-isoxazole	H	CH(Ph)O	91.2±5.7	-
36c	N-Me-pyrazole	H	CH(Ph)O	74.7±7.81	-
Nitrogen-linked analogs					
40				20.8	-
41				1.6±0.2	-
Pyrrolidine cyanamides					
42				26.4±1.1	-
43				315±17.6	-

^a IC₅₀s performed in triplicate and determined from eight concentrations in the hNAAA inhibition assay. Activity measured after 90 min pre-incubation of the inhibitor and enzyme prior to the addition of the fluorogenic substrate N-(4-methyl coumarin) palmitamide (PAMCA). IC₅₀ values were calculated using Prism software (GraphPad).

In order to address the weak selectivity profile of this new class of NAAA inhibitors, we have introduced steric/bulky groups with relative and absolute configuration, as well as conformational restriction at the vicinity of the azetidine-nitrile pharmacophore. Conformational restriction at this part of the ligand represents a rational optimization approach to interrogate potency and selectivity by targeting additional van der Waals contacts to improve potency and also to create discriminatory ligand/protein interactions with residues against other cysteine proteases and serine hydrolases and enhance ligand selectivity for the target. As we briefly discussed above, our molecular modeling studies (Fig. 4) with the hNAAA X-ray structure revealed the presence of a hydrophobic cavity (formed by residues Phe174, Trp181, Tyr146) at the vicinity of the benzylic position (linker region) of compound **17f**. To take advantage of this unoccupied region, we have introduced substituents on the molecule projecting toward this hydrophobic cavity of the binding pocket to fill the space and influence potency and selectivity for the target. To that end, we have introduced substitutions on the ligand as followed:

1). Introduced *ortho*-position substitutions on the proximal-phenyl group (Table 1). The fluoro (**17o**) and trifluoromethyl (**17p**) analogs showed comparable potency to that of **17d**, while the methoxy analog **17q** was about 3-fold weaker.

Next, we introduced an oxygen atom between the two phenyl groups (phenoxy analog **23**), which offered a higher degree of rotational flexibility than the parent biphenyl analog **17a**. Analog **23** was about 3-fold more potent than **17a**. Introduction of bulkier substituents at the *ortho*-position of **23** shown in entries **24**, **25a-25e** (Table 1) exhibited a varied degree of potency for NAAA with IC₅₀ values in the range of 1-24 nM. The bromo-analog **24** was the most potent analog with an IC₅₀ value of 1 nM, while the phenyl (**25a**) and 2-OMe-phenyl (**25b**) analogs were weaker with 8-fold and 22-fold potency loss, respectively. The remaining analogs **25c-25e** showed a small reduction in potency. While the *ortho*-introduced modifications produced potent inhibitors for NAAA, they only marginally improved the selectivity (~ 10-20-fold) of the molecule against FAAH and MGL.

2). Added substituents at the benzylic-position of ligand **17d** (Table 1). We have considered that such modifications would have been beneficial to the molecule by masking the benzylic position from any potential CYP-450 oxidative liability. We introduced a phenyl substituent (entry **36a**) at the benzylic position, but unfortunately it was not well tolerated and resulted in about 12-fold drop in ligand potency (**36a** vs **17d**). Replacement of the distal phenyl of **36a** with polar groups (entries **36b** and **36c**) has caused even a larger loss in potency.

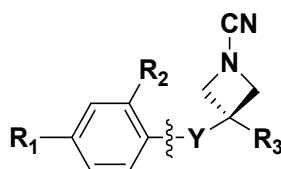
3). Constrained the methoxy-linker of **17f** with the preparation of a fused-isoindoline ring (**41**, Table 1). This new bicyclic motif exhibited high potency for NAAA with an IC₅₀ value of 1.6 nM, but still lacked good selectivity against the serine hydrolases FAAH and MGL.

4). Prepared 3,3 di-substituted-azetidine analogs (Table 2).

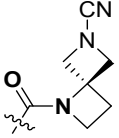
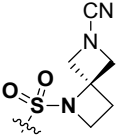
First, we introduced a small methyl group (entry **30a**) which exhibited 2-fold loss in potency (IC₅₀ = 1.8 nM) when compared to the monosubstituted analog **17d** (Table 1), however it was gratifying to observe that **30a** was highly selective (~500-fold) against hMGL. Analog **30a** also exhibited an improved selective profile against cathepsin K (~50-fold; data not shown). Unfortunately, **30a** showed no improvement in selectivity against hFAAH. The bulkier phenyl group (analog **30b**) was about 4-fold weaker (IC₅₀ = 9.1 nM) than the methyl analog **30a** for hNAAA, showed good selectivity (>100-fold) against MGL, but still lacked selectivity against FAAH (~ 6 fold). Modifications of the distal phenyl of **30b** with polar moieties, dioxole (**30c**) and dioxine (**30d**)

were tolerated with IC_{50} values of 9.2 and 6.1 nM, respectively. The meta-pyridyl analog **30e** has retained the hNAAA potency ($IC_{50} = 4.6$ nM), while the cyclopropane **30f** analog was found to be the most potent hNAAA inhibitor with an IC_{50} value of 0.35 nM. Induced-fit docking of **30f** with the hNAAA crystal structure (Fig. 6) revealed that the cyclopropane group of **30f** was buried into the unoccupied hydrophobic cavity formed by residues Trp181, Tyr146, and Phe174 (not shown). Hydrophobic van der Waals interactions between the cyclopropane ring and the hydrophobic residues of this hydrophobic cavity could account for the enhanced affinity of **30f**.

Table 2. Di-substituted cyanamides hNAAA inhibitors



Compd	R ₁	R ₂	R ₃	Y	IC ₅₀ (nM) ± SD ^a or % inhibition @ 1 uM		
					hNAAA	hFAAH	hMGL
3,3-Di-substituted azetidines							
30a	3-OMePh	H	Me	CH ₂ O	1.8±0.3	0.36±0.02	1058±47
30b	3-OMePh	H	Ph	CH ₂ O	9.1±0.6	61±4	19.5%
30c	benzo[d][1,3]dioxole	H	Ph	CH ₂ O	9.2±0.9	99%	59%
30d	2,3-dihydrobenzo[b][1,4]dioxine	H	Ph	CH ₂ O	6.1±0.8	99%	13.5%
30e	4-OMe,3F-Ph	F	<i>m</i> -pyridyl	CH ₂ O	4.6±0.4	2.0±0.2	66%
30f	4-OMe,3F-Ph	F	cyclopropane	CH ₂ O	0.35±0.03	1.0±0.3	472±87
49	3-OMePh	H	Me	CONH	1.58±0.08	23%	11%
50	3-OMePh	H	Me	SO ₂ NH	3.2±0.2	17.8±2.2	19%
3,3-Spiro-azetidines							

51	3-OMePh	H		6.5±0.4	6%	4%
52	3-OMePh	H		2.8±0.1	10.2±1.9	14%

^a IC₅₀s performed in triplicate and determined from eight concentrations in the hNAAA inhibition assay. Activity measured after 90 min pre-incubation of the inhibitor and enzyme prior to the addition of the fluorogenic substrate N-(4-methyl coumarin) palmitamide (PAMCA). IC₅₀ values were calculated using Prism software (GraphPad).

Next, to further restrict the conformational flexibility of the azetidine nucleus attached to the proximal-phenyl group, we have replaced the methoxy-linker of **30a** with amide or sulfonamide moieties. The amide-linked analog **49** was found to be highly potent for hNAAA (IC₅₀ = 1.58 nM) and gratifyingly exhibited good selectivity (>100-fold) against all tested enzymes hFAAH, hMGL,

hABHD6 and cathepsin K. The analogous sulfonamide **50** was found to be 2-fold less potent than the amide **49**. Interestingly, the sulfonamide **50** has retained good selectivity (>100-fold) against hMGL, hABHD6 and cathepsin K, but showed a strong inhibitory activity for hFAAH (IC₅₀ = 18 nM).

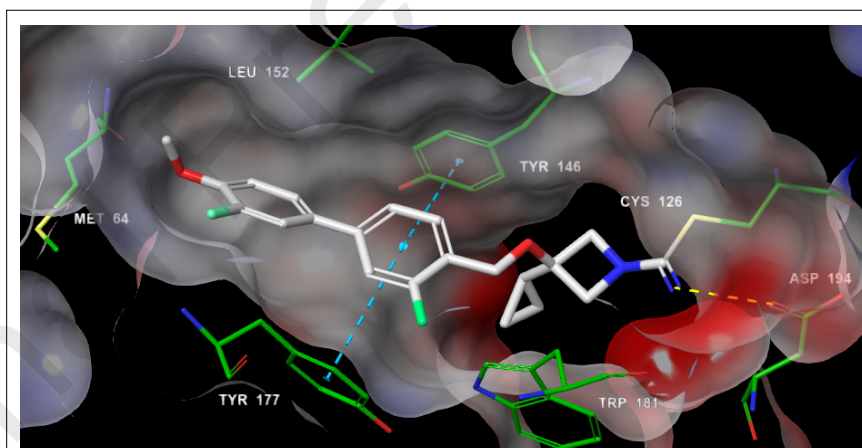


Fig. 6 Induced-fit docking of **30f** (Table 2) with hNAAA crystal structure. A Connolly surface shown as electrostatic potential (red-white-blue) was used to represent the shape of the binding pocket. Only the key residues (green) and the ligand (white) are shown. All other atoms are colored by atom type. The ligand orients into the binding pocket making several π -stacking interactions shown in blue dashed lines. Hydrogen bonds are indicated by yellow dashed lines.

5). Prepared 3,3 spiro-azetidine analogs (Table 2).

Next, we added additional conformational restriction at the azetidine nucleus of **49** and **50** to further influence the ligand selectivity for the target. Both spiro[3.3]heptane analogs **51** (amide-

linker) and **52** (sulfonamide-linker) were potent inhibitors for hNAAA with IC_{50} values of 6.5 and 2.8 nM, respectively. Again, only the amide analog **51** showed good selectivity (>100-fold) against serine hydrolases hFAAH, hMGL, hABHD6 and cysteine peptidase cathepsin K, while the sulfonamide analog **52** was found to be highly potent for both hNAAA ($IC_{50} = 2.8$ nM) and FAAH ($IC_{50} = 10.2$ nM) and selective (>100-fold) against MGL, ABHD6 and cathepsin K, in agreement with the analogous sulfonamide **50**.

We have concluded that the amide-linked inhibitors were highly potent ($IC_{50} < 10$ nM) for hNAAA and selective (>100-fold) against serine hydrolases, hFAAH, hMGL and hABHD6 and cysteine peptidase cathepsin K. In contrast, the sulfonamide-linked inhibitors showed potent dual inhibition for hNAAA and hFAAH and good selectivity (>100-fold) against hydrolases hMGL, and hABHD6 and peptidase cathepsin K. A very recent report⁶⁴ outlined the utility of dual NAAA-FAAH inhibitors as a potential therapeutic approach for acute lung injury (ALI) due to inflammatory progression. We believe that the dual NAAA-FAAH inhibitors represent an exciting new anti-inflammatory pharmacological approach by potentially combining two distinct molecular anti-inflammatory pathways, first, NAAA inhibitors to augment the PEA/PPAR- α anti-inflammatory signaling pathway¹⁻⁴, and secondly FAAH inhibitors to increase the endocannabinoid anandamide (AEA) levels which activates the cannabinoid receptors CB1 and CB2, both known for their strong anti-inflammatory and antinociceptive properties⁵⁻⁸.

3.1 Compound properties: We have evaluated a small set of potent ($IC_{50} < 10$ nM) cyanamides in stability assays.

3.1.1 Plasma and gastric fluids stability: The tested cyanamides exhibited good plasma stability ($t_{1/2} > 2$ hours) in human and rat plasma and in gastric fluids (Table 3).

Table 3. Plasma and gastric fluids stability of cyanamides hNAAA inhibitors

Compd	Plasma stability $t_{1/2}$ min		Gastric fluids stability $t_{1/2}$ min
	Human	Rat	
17d	204	189	450
17o	228	184	271
30f	127	-	-
49	902	-	-
50	221	-	-
51	458	-	-
52	180	-	-

Table 4. Microsomal stability of cyanamides hNAAA inhibitors

Compd	Microsomal stability $t_{1/2}$ min	
	Human	Rat
17d	11.2	10
17j	6.8	8.9
17o	5.7	7.9
30b	15.3	14.5
40	11.3	-
41	14.7	4.4

3.1.2 Microsomal stability: The microsomal stability ($t_{1/2}$, min) of the tested cyanamides in human and rat liver microsomal preparations was moderate with $t_{1/2}$ values in the range of 5 to 15 min (Table 4).

The new discovered cyanamides, encompassing both potent NAAA inhibitors and potent dual NAAA-FAAH inhibitors represent promising pharmacological tools to investigate their potential role in anti-inflammatory and pain preclinical models. Their pharmacological evaluation in preclinical models of inflammation and pain will be presented elsewhere in due course.

4. Conclusions

NAAA inhibition represents an exciting novel approach to treat inflammatory conditions supported by recent publications^{1-4, 30}. In this report, we have described the exploration of the cyanamide moiety as a new pharmacophore for NAAA inhibition that led to the discovery of highly potent and selective inhibitors. Key analogs demonstrated single-digit nanomolar potency for hNAAA and showed >100-fold selectivity for the serine hydrolases FAAH, MGL and ABHD6, and cysteine protease cathepsin K. We have also identified potent and selective dual NAAA-FAAH inhibitors, which combine two distinct anti-inflammatory molecular pathways by activating the PEA/PPAR- α anti-inflammatory signaling pathway¹⁻⁴ via NAAA inhibition, and also stimulating the cannabinoid receptors CB1 and CB2 via augmentation of the endocannabinoid AEA through FAAH inhibition. Both CB1 and CB2 receptors are known for their anti-inflammatory and antinociceptive properties⁵⁻⁸. Our ligand design followed a traditional structure-activity relationship (SAR) approach and was supported by molecular modeling studies of the reported X-ray cocrystal structures of NAAA⁵⁰. Several inhibitors were evaluated in stability assays and demonstrated very good plasma stability ($t_{1/2}$ >120 min; human and rodents), but rather moderate microsomal stability ($t_{1/2}$ ~5-15 min) in human and rodent liver microsomal preparations. The disclosed cyanamides represent promising new pharmacological tools to investigate the potential role of NAAA inhibitors and dual NAAA-FAAH inhibitors as therapeutic agents for the treatment of inflammation and pain.

5. Experimental section

5.1. Chemistry

All solvents and reagents were obtained from commercial sources and were used as received. All non-aqueous reactions were carried out in oven-dried glassware under an atmosphere of dried argon or nitrogen. All reactions were monitored by thin layer chromatography (TLC plates F254, Merck) or LC-MS analysis. All products, unless otherwise noted, were purified by flash chromatography by Biotage Isolera purification system using pre-packed silica cartridges. Proton nuclear magnetic resonance spectra were obtained on a VARIAN 400 spectrometer at 500 MHz. Spectra are given in ppm (δ) and coupling constants, J values, are reported in hertz. Splitting patterns are designated as follows: s, singlet; brs, broad singlet; d, doublet; t, triplet; q, quartet; m, multiplet. Tetramethylsilane was used as an internal reference standard. Mass spectra were obtained on a Waters Micromass ZQ spectrometer. HPLC techniques and mass spectrometry were used to determine the purity of the compounds. Purity of all final products was > 96% as determined by LC-MS using the following protocol. Mobile Phase A = water, B = acetonitrile solvent gradient 95/5 to 5/95 A:B in 11 min; flow rate 1.5 mL/min; Waters XTerra MS C8 column (4.6 \times 50 mm) with UV detection at 190-400 nm wavelength.

5.1.1 Method A (scheme 1).

5.1.1.1 *tert*-Butyl 3-((4-bromobenzyl)oxy)azetidine-1-carboxylate (**14**, $X = \text{CH}_2\text{O}$, $R_2 = \text{H}$).

Step b). Sodium hydride (60% dispersion in mineral oil; 663.2 mg, 16.58 mmol) was added portionwise into a cold (0 °C) solution of *tert*-butyl 3-hydroxyazetidine-1-carboxylate (**3**, 2.38 g, 13.82 mmol) and DMF (20 mL). After stirring for 1 hour, 1-bromo-4-(bromomethyl)benzene (3.8 g, 15.2 mmol) was added and the new mixture was allowed to come to room temperature and stirred for 12 h. The mixture was then cooled to 0 °C and MeOH (4 mL) was added dropwise. Afterwards, the mixture was poured into aqueous ammonium chloride and extracted twice with ethyl ether. The organic extracts were dried over anhydrous MgSO_4 . The solvents were removed under vacuum and the residue was purified on silica gel (Biotage; eluting solvents hexanes: EtOAc 4/1 ratio) to afford *tert*-butyl 3-((4-bromobenzyl)oxy) azetidine-1-carboxylate as off-white solid (4.32 g, 92% yield): ^1H NMR (500MHz, CDCl_3) δ ppm 7.47 (d, $J = 8$ Hz, 2H), 7.20 (d, $J = 8$ Hz, 2H), 4.41 (s, 2H), 4.28 (m, ^1H), 4.05 (dd, $J = 8.5, 5.0$ Hz, 2H), 3.85 (dd, $J = 8.5, 5.0$ Hz, 2H), 1.41 (s, 9H); MS (ES) m/z 343.1288 $[\text{M}+1]^+$.

5.1.1.2 *tert*-Butyl 3-((4'-methoxy-[1,1'-biphenyl]-4-yl)methoxy)azetidine-1-carboxylate (**15**, $R_1 = 4\text{-OMePh}$, $R_2 = H$, $X = \text{CH}_2\text{O}$).

Step c). Into a microwave vessel were added *tert*-butyl 3-((4-bromobenzyl)oxy)azetidine-1-carboxylate (200 mg, 0.58 mmol), (4-methoxyphenyl)boronic acid (177 mg, 1.16 mmol), K_2CO_3 (240 mg, 1.74 mmol), dioxane (8 mL) and water (2 mL). Argon gas was passed through the mixture for 10 minutes and then tetrakis(triphenylphosphine)palladium(0) (6.7 mg 0.0058 mmol) and the argon flow continued for 5 additional minutes. Then, the vessel was sealed and microwaved at 100 °C for 1 h. The mixture was diluted with EtOAc (30 mL) and washed with water and brine. The organics extracts were dried over anhydrous MgSO_4 . The solvents were removed under vacuum and the residue was purified on silica gel (Biotage; eluting solvents hexanes: EtOAc 4/1 ratio) to afford *tert*-butyl 3-((4'-methoxy-[1,1'-biphenyl]-4-yl)methoxy)azetidine-1-carboxylate as viscous oil (189 mg, 88% yield): ^1H NMR (500MHz, CDCl_3) δ ppm 7.53 (d, $J = 8.0$ Hz, 2H), 7.51 (d, $J = 8.5$ Hz, 2H), 7.38 (d, $J = 8.0$ Hz, 2H), 6.95 (d, $J = 8.5$ Hz, 2H), 4.47. (s, 2H), 4.33 (m, ^1H), 4.08 (dd, $J = 8.5, 5.0$ Hz, 2H), 3.85 (dd, $J = 8.5, 5.0$ Hz, 2H), 1.41 (s, 9H). MS (ES) m/z 370.2211 $[\text{M}+1]^+$.

5.1.1.3. 3-((4'-Methoxy-[1,1'-biphenyl]-4-yl)methoxy)azetidine.TFA salt (**16**, $R_1 = 4\text{-OMePh}$, $R_2 = H$, $X = \text{CH}_2\text{O}$).

Step d). Trifluoroacetic acid (0.36 mL, 4.7 mmol) was added into a mixture of *tert*-butyl 3-((4'-methoxy-[1,1'-biphenyl]-4-yl)methoxy)azetidine-1-carboxylate (175 mg, 0.47 mmol) and CH_2Cl_2 (10 mL). The mixture was stirred at room temperature for 6 h and then the volatiles were removed under vacuum. The residue was taken (3x) successively in CHCl_3 (10 mL) and the volatiles were removed under vacuum to ensure removal of excess TFA. The crude 3-((4'-methoxy-[1,1'-biphenyl]-4-yl)methoxy)azetidine.TFA salt (180 mg) was carried to the next step.

5.1.1.4. 3-((4'-Methoxy-[1,1'-biphenyl]-4-yl)methoxy)azetidine-1-carbonitrile (compound **17f**, $R_1 = 4\text{-OMePh}$, $R_2 = H$, $X = \text{CH}_2\text{O}$; Table 1). Step e). Triethylamine (0.33 mL, 2.35 mmol) was added into a cold (0 °C) mixture of 3-((4'-methoxy-[1,1'-biphenyl]-4-yl)methoxy)azetidine.TFA salt (180 mg, 0.47 mmol), and CH_2Cl_2 (8 mL). After stirring for 30 minutes cyanogen bromide (99.5 mg, 0.94 mmol) was added and the mixture was allowed to come to room temperature and stirred for 4 h. Then, the mixture was diluted in EtOAc (30 mL) and washed with water and brine.

The organics extracts were dried over anhydrous MgSO_4 . The solvents were removed under vacuum and the residue was purified on silica gel (Biotage; eluting solvents hexanes: EtOAc 3/1 ratio) to afford 3-((4'-methoxy-[1,1'- biphenyl]-4-yl)methoxy)azetidine-1-carbonitrile as white solid (112 mg, 81% yield): $^1\text{H NMR}$ (500MHz, CDCl_3) δ ppm 7.55 (d, $J = 8$ Hz, 2H), 7.51 (d, $J = 8.5$ Hz, 2H), 7.34 (d, $J = 8$ Hz, 2H), 6.97 (d, $J = 8.5$ Hz, 2H), 4.47. (s, 2H), 4.41 (m, ^1H), 4.24 (dd, $J = 8.5, 5.0$ Hz, 2H), 4.11 (dd, $J = 8.5, 5.0$ Hz, 2H); MS (ES) m/z 295.4289 $[\text{M}+1]^+$; purity 98.5%, retention time 4.71 min.

5.1.1.5. *tert*-Butyl 3-(hydroxymethyl)azetidine-1-carboxylate (**11**; scheme 1).

Step a). Sodium borohydride (756 mg, 20 mmol) was added portionwise into a solution of 1-(*tert*-butyl) 3-methyl azetidine-1,3-dicarboxylate (2.11 g, 10 mmol) and THF (10 mL). The mixture was heated to 80 °C and then MeOH (2 mL) was added very slowly over a 30 minute period. The mixture was stirred for 1 hour, cooled to room temperature and poured slowly into ice-cold HCl (0.5 N). The mixture was extracted (3x) with EtOAc and the organic extracts were dried over anhydrous MgSO_4 . The solvents were removed under vacuum and the residue was purified on silica gel (Biotage; eluting solvents hexanes: EtOAc 2/1 ratio) to afford *tert*-butyl 3-(hydroxymethyl)azetidine-1-carboxylate as oil (1.69 g, 90% yield): $^1\text{H NMR}$ (500MHz, CDCl_3) δ ppm 3.98 (t, $J = 8.3$, 2H), 3.77 (m, 2H), 3.68 (dd, $J = 8.77, 5.37$ Hz, 2H), 2.7 (m, ^1H); MS (ES) m/z 188.2144 $[\text{M}+1]^+$.

5.1.1.6. 3-((*[1,1'*-Biphenyl]-4-ylmethoxy)methyl)azetidine-1-carbonitrile (compound **17c**, $X = \text{O}$; $R_2 = \text{H}$; Table 1).

This compound was prepared according to Method A, steps b-e). $^1\text{H NMR}$ (500MHz, CDCl_3) δ ppm 7.6 (m, 4H), 7.44 (m, 2H), 7.39 (m, 3H), 4.21 (t, $J = 7.81$, Hz, 2H), 4.0 (dd, $J = 7.81, 5.86$ Hz, 2H), 3.6 (d, $J = 6.35$ Hz, ^1H), 2.98 (m, ^1H); MS (ES) m/z 279.4424 $[\text{M}+1]^+$; purity 99.5%, retention time 4.75 min.

5.1.2 Method B (scheme 2).

5.1.2.1. 2-Bromo-4-phenoxybenzaldehyde (**19**).

Step a). Potassium carbonate (5.98 g, 43.28 mmol) was added into a mixture of phenol (2.31 g, 24.6 mmol), 2-bromo-4-fluorobenzaldehyde (5g, 24.6 mmol) and DMF (50 mL). The mixture was

stirred at 100 °C for 18 hours, cooled to room temperature and then poured into water (200 mL). The mixture was stirred for 30 minutes and the precipitated solid filtered and washed with water. 2-Bromo-4-phenoxybenzaldehyde as an off-white solid (6.15 g, 90% yield) was collected and used to the next step. ¹H NMR (500MHz, CDCl₃) δ ppm 10.24 (s, 1H), 7.9 (d, *J* = 9.0 Hz, 1H), 7.45-7.42 (m, 2H), 7.27 (t, *J* = 7.5 Hz, 1H), 7.17 (d, *J* = 2.5 Hz, 1H), 7.09-7.08 (m, 2H), 6.98 (dd, *J* = 9.0, 2.5 Hz, 1H).

5.1.2.2. (2-Bromo-4-phenoxyphenyl) methanol (21a).

Step b). Sodium borohydride (544.3 mg, 14.4 mmol) was added in portions into a cold (0 °C) mixture of 2-bromo-4-phenoxybenzaldehyde (6.25 g, 22.56 mmol) and anhydrous methanol (30 mL). After the addition the mixture stirred for 30 minutes, and then it was carefully poured into ice water. The mixture was extracted with ethyl acetate and the organic extracts washed with water and brine and dried over anhydrous MsSO₄. The solvents were removed under vacuum and the residue was purified on silica gel (Biotage; eluting solvents hexanes: EtOAc 3/1 ratio) to afford (2-bromo-4-phenoxyphenyl)methanol as oil (5.92 g, 94.4% yield): ¹H NMR (500MHz, CDCl₃) δ ppm 7.42 (d, *J* = 8.5 Hz, 1H), 7.38-7.34 (m, 4H), 7.2 (d, *J* = 2.5 Hz, 1H), 7.16 (t, *J* = 7.5 Hz, 1H), 7.0 (dd, *J* = 8.5, 2.5 Hz, 1H), 4.71 (d, *J* = 6.5 Hz, 2H), 1.97 (t, *J* = 6.5 Hz, 1H).

5.1.2.3. 2-Bromo-1-(bromomethyl)-4-phenoxybenzene (21b).

Phosphorus tribromide (4.3 mL, 44.74 mmol) was added dropwise into a cold (0 °C) mixture of (2-bromo-4-phenoxyphenyl) methanol (4.9 g, 17.56 mmol) and anhydrous tetrahydrofuran (50 mL). After the addition the mixture stirred at room temperature for 5 hours, and then it was carefully poured into ice water. The mixture was extracted with ethyl acetate and the organic extracts washed with saturated aqueous sodium bicarbonate (three times), water and brine and dried over anhydrous MgSO₄. The solvents were removed under vacuum and the residue was purified on silica gel (Biotage; eluting solvents hexanes: EtOAc 30/1 ratio) to afford 2-bromo-1-(bromomethyl)-4-phenoxybenzene as oil (4.26 g, 71% yield): ¹H NMR (500MHz, CDCl₃) δ ppm 7.4-7.36 (m, 3H), 7.19-7.16 (m, 2H), 7.04-7.03 (m, 2H), 6.92 (dd, *J* = 8., 2.5 Hz, 1H), 4.6 (s, 2H).

5.1.2.4. 3-((2-Bromo-4-phenoxybenzyl)oxy)azetidine-1-carbonitrile (compound 24; Table 1).

This compound was prepared according to Method A, steps b-e). ^1H NMR (500MHz, CDCl_3) δ ppm 7.39-7.34 (m, 3H), 7.19 (d, $J = 2.5$ Hz, 1H), 7.17 (t, $J = 7.5$ Hz, 1H), 7.03-7.0 (m, 2H), 6.97 (dd, $J = 8.0, 2.5$ Hz, 1H), 4.48 (s, 2H), 4.46-4.43 (m, 1H), 4.3-4.27 (m, 2H), 4.16-4.13 (m, 2H); MS (ES) m/z 361.3470 $[\text{M}+1]^+$; purity 98%, retention time 5.01 min.

5.1.2.5. *3-((5-Phenoxy-[1,1'-biphenyl]-2-yl)methoxy)azetidine-1-carbonitrile* (compound 25; Table 1).

Step f.) Into a microwave vessel were added 3-((2-bromo-4-phenoxybenzyl)oxy)azetidine-1-carbonitrile (120 mg, 0.33 mmol), phenylboronic acid (60.4 mg, 0.49 mmol), cesium fluoride (100.3 mg, 0.66 mmol) and anhydrous dimethoxyethane (4 mL). Dry argon gas was passed through the mixture for 10 minutes and then tetrakis(triphenylphosphine)palladium(0) (12.4 mg 0.0099 mmol) was added and the argon flow continued for 5 additional minutes. Then, the vessel was sealed and microwaved at 100 °C for 1 hour. The mixture was diluted with EtOAc (30 mL) and washed with water and brine. The organics extracts were dried over anhydrous MgSO_4 . The solvents were removed under vacuum and the residue was purified on silica gel (Biotage; eluting solvents hexanes: EtOAc 3/1 ratio) to afford 3-((5-phenoxy-[1,1'-biphenyl]-2-yl)methoxy)azetidine-1-carbonitrile as oil (94.6 mg, 79% yield): ^1H NMR (500MHz, CDCl_3) δ ppm 7.44-7.39 (m, 4H), 7.38-7.31 (m, 4H), 7.14 (dt, $J = 7.5$ Hz, 1.5 Hz, 1H), 7.07-7.05 (m, 2H), 7.01 (dd, $J = 8.0, 2.5$ Hz, 1H), 6.94 (d, $J = 2.5$ Hz, 1H), 4.26 (s, 2H), 4.25-4.2 (m, 1H), 4.14-4.11 (m, 2H), 3.94-3.91 (m, 2H); MS (ES) m/z 357.4797 $[\text{M}+1]^+$; purity 98%, retention time 5.18 min.

5.1.3 Method C (scheme 3).

5.1.3.1. *tert-Butyl 3-hydroxy-3-methylazetidine-1-carboxylate* (27, $R_3 = \text{methyl}$; scheme 3).

Step a). Methyl magnesium bromide (3M in diethyl ether; 2.92 mL, 8.76 mmol) was added portionwise into a cold (0 °C) solution of *tert*-butyl 3-oxoazetidine-1-carboxylate (0.5 g, 2.92 mmol) and anhydrous THF (3 mL). The mixture was allowed to come to room temperature and stirred for 3 hours and carefully quenched with aqueous ammonium chloride. The mixture was extracted with ethyl acetate, washed with brine and dried over anhydrous MgSO_4 . The solvents were removed under vacuum and the residue was purified on silica gel (Biotage; eluting solvents hexanes: EtOAc 1/1 ratio) to afford *tert*-butyl 3-hydroxy-3-methylazetidine-1-carboxylate as oil

(480 mg, 87% yield): $^1\text{H NMR}$ (500MHz, CDCl_3) δ ppm 3.87 (d, $J = 9.0$ Hz, 2H), 3.82 (d, $J = 9.0$, 2H), 2.46 (s, 1H), 1.51 (s, 3H), 1.44 (s, 9H).

5.1.3.2. *tert*-Butyl 3-((4-bromobenzyl)oxy)-3-methylazetidine-1-carboxylate (**28**, $R_2 = \text{H}$, $R_3 = \text{Me}$; scheme 3)

Step b). Into a mixture of *tert*-butyl 3-hydroxy-3-methylazetidine-1-carboxylate (480 mg, 2.56 mmol), 1-bromo-4-(bromomethyl)benzene and dichloromethane (5 mL) were added NaOH (4N, 6 mL) and tetra-*n*-butylammonium bromide (82.6 mg, 0.256 mmol). The mixture was refluxed for 16 hours, cooled to room temperature and extracted with ethyl ether. The organic extracts were washed with water and brine and dried over anhydrous MgSO_4 . The solvents were removed under vacuum and the residue was purified on silica gel (Biotage; eluting solvents hexanes: EtOAc 3/1 ratio) to afford *tert*-butyl 3-((4-bromobenzyl)oxy)-3-methylazetidine-1-carboxylate as oil (826 mg, 90.5% yield): $^1\text{H NMR}$ (500MHz, CDCl_3) δ ppm 7.48 (d, $J = 8.5$ Hz, 2H), 7.22 (d, $J = 8.5$ Hz, 2H), 4.38 (s, 2H), 3.98 (d, $J = 9.5$ Hz, 2H), 3.74 (d, $J = 9.5$ Hz, 2H), 1.55 (s, 3H), 1.44 (s, 9H).

5.1.3.3. 3-((3'-Methoxy-[1,1'-biphenyl]-4-yl)methoxy)-3-methylazetidine-1-carbonitrile (compound **30a**; Table 2).

This compound was prepared according to Method A, steps b-e). $^1\text{H NMR}$ (500MHz, CDCl_3) δ ppm 7.59 (d, $J = 8.0$ Hz, 2H), 7.40 (d, $J = 8.0$ Hz, 2H), 7.36 (t, $J = 8.9$ Hz, 1H), 7.18-7.16 (m, 1H), 7.12-7.11 (m, 1H), 6.91-6.89 (m, 1H), 4.46 (s, 2H), 4.26 (d, $J = 8.5$ Hz, 2H), 3.94 (d, $J = 8.5$ Hz, 2H), 3.87 (s, 3H), 1.64 (s, 3H); MS (ES) m/z 309.4735 $[\text{M}+1]^+$; purity 98%, retention time 4.82 min.

5.1.4 Method D (scheme 4).

5.1.4.1. 1-Benzhydryl-3-((4-bromophenyl)(phenyl)methoxy)azetidine (**34**).

Step a). A mixture of 1-benzhydrylazetidin-3-ol 94.54 g, 19.0 mmol), (4-bromophenyl)(phenyl)methanol (5.9 g, 19.0 mmol), dichloromethane (50 mL) and *p*-toluenesulfonic acid (6.5 g, 38 mmol) was refluxed for 1 h under continuous removal of water with a Dean-Stark trap. The mixture cooled to room temperature, poured into water and extracted with ethyl acetate. The organic extracts were washed with water and brine and dried over anhydrous MgSO_4 . The solvents were removed under vacuum and the residue was purified on silica gel

(Biotage; eluting solvents hexanes: EtOAc 10/1 ratio) to afford 1-benzhydryl-3-((4-bromophenyl)(phenyl)methoxy)azetidine as oil (5.1 g, 55.5% yield): ^1H NMR (500MHz, CDCl_3) δ ppm 7.41-7.4 (m, 2H), 7.36-7.34 (m, 4H), 7.3-7.24 (m, 2H), 7.26-7.22 (m, 7H), 7.18-7.14 (m, 4H), 5.23 (s, 1H), 4.33 (s, 1H), 4.02-4.17 (m, 1H), 3.44-3.36 (m, 2H), 2.94-2.9 (m, 2H).

5.1.4.2. 3-((4-Bromophenyl)(phenyl)methoxy)azetidine hydrochloride (35).

Step b). 1-Chloroethyl chloroformate (3.69 g, 25.82 mmol) was added to a cold (0 °C) mixture of 1-benzhydryl-3-((4-bromophenyl)(phenyl)methoxy)azetidine (5.0 g, 10.33 mmol), and dichloromethane (50 mL). The mixture was allowed to come to room temperature and stirred for 20 hours. The volatiles were removed under vacuum and the residue was dissolved in methanol and stirred for 1 hour. The methanol removed under vacuum and the crude product (3.68 g) was used to the next step.

The following compounds were prepared according to Method C.

5.1.4.3. 3-((3'-Methoxy-[1,1'-biphenyl]-4-yl)(phenyl)methoxy)azetidine-1-carbonitrile (compound 36a; Table 1).

This compound was prepared according to Method B, steps e-f). ^1H NMR (500MHz, CDCl_3) δ ppm 7.56 (d, $J = 8.0$ Hz, 2H), 7.37-7.33 (m, 8H), 7.15(dd, $J = 8.5, 1.0$ Hz, 1H), 7.09 (t, $J=2\text{Hz}$, 1H), 6.09 (dd, $J = 8.5, 2.5$ Hz, 1H), 5.35 (s, 1H), 4.46-4.44 (m, 1H), 4.16-4.14 (m, 2H), 4.11 (m, 2H), 3.86 (s, 3H); MS (ES) m/z 371.5464 $[\text{M}+1]^+$; purity 99.5%, retention time 5.15 min.

5.1.5 Method E (scheme 5).

5.1.5.1. tert-Butyl 3-((1,1'-biphenyl]-4-ylmethyl)(methyl)amino)azetidine-1-carboxylate (38a, $R_4 = \text{Ph}$, $Y = \text{none}$).

Step a). Into a mixture of 1-([1,1'-biphenyl]-4-yl)-N-methylmethanamine hydrochloride (254 mg, 1.09 mmol), *tert*-butyl 3-oxoazetidine-1-carboxylate (169.6 mg, 0.99 mmol), acetic acid (0.17 mL) and anhydrous tetrahydrofuran (3 mL), was added sodiumtriacetoxy borohydride (292 mg, 1.39 mmol). The mixture was stirred for 5 hours and then was quenched with saturated aqueous sodium bicarbonate. The mixture was extracted with ethyl acetate, washed with brine and dried over anhydrous MgSO_4 . The solvents were removed under vacuum and the residue was purified on

silica gel (Biotage; eluting solvents hexanes: EtOAc 2/1 ratio) to afford *tert*-butyl 3-((1,1'-biphenyl]-4-ylmethyl)(methyl)amino)azetidine-1-carboxylate as oil (326 mg, 84.9% yield): ^1H NMR (500MHz, CDCl_3) δ ppm 7.59 (d, $J = 7.5$ Hz, 2H), 7.56 (d, $J = 7.5$ Hz, 2H), 7.4 (m, 2H), 7.36-7.34 (m, 3H), 3.97-3.94 (m, 2H), 3.88-3.85 (m, 2H), 3.43 (s, 2), 3.3-3.26 (m, 1H), 2.1 (s, 3H), 1.45 (s, 9H).

5.1.5.2. 3-((1,1'-Biphenyl]-4-ylmethyl)(methyl)amino)azetidine-1-carbonitrile (compound 40; Table 1).

This compound was prepared according to Method A, steps c-e). ^1H NMR (500MHz, CDCl_3) δ ppm 7.6-7.58 (m, 2H), 7.56 (d, $J = 8.0$, 2H), 7.46 (t, $J = 8.0$ Hz, 2H), 7.36-7.33 (m, 3H), 4.13-4.08 (m, 4H), 3.49 (m, 1H), 3.43 (s, 2H), 2.13 (s, 3H) MS (ES) m/z 278.4513 $[\text{M}+1]^+$; purity 100%, retention time 4.71 min.

5.1.6 Method F (scheme 6).

5.1.6.1. *Tert*-butyl 3-(3'-methoxy-[1,1'-biphenyl]-4-carboxamido)azetidine-1-carboxylate (45, Z = CO; scheme 6).

Step a). To a stirred solution of 3'-methoxy-[1,1'-biphenyl]-4-carboxylic acid (228 mg, 1 mmol), and *tert*-butyl 3-amino-3-methylazetidine-1-carboxylate (189.2 mg, 1.02 mmol) and *N,N*-diisopropyl-ethylamine (452.4 mg, 3.5 mmol) in DMF (5 mL) was added HBTU (1.32g, 3.48 mmol). The resulting mixture was stirred at room temperature for 18 hours. The reaction mixture was partitioned between water (30 mL) and ethyl acetate (30 mL) and the aqueous layer was extracted with ethyl acetate (50 mL). The combined organic extracts were washed with saturated NaHCO_3 (30 mL), and brine (30 mL). The organic layer was dried over Na_2SO_4 and concentrated under reduced pressure. The residue was purified on silica gel (Biotage; eluting solvents hexane: EtOAc 4/1 ratio) to afford *tert*-butyl 3-(3'-methoxy-[1,1'-biphenyl]-4-carboxamido)-3-methylazetidine-1-carboxylate as a colorless solid in 80% yield; ^1H NMR (500 MHz, CDCl_3) δ 7.83 (d, $J = 8.4$ Hz, 2H), 7.59 (d, $J = 8.3$ Hz, 2H), 7.34 (t, $J = 7.9$ Hz, 1H), 7.15 (d, $J = 7.7$ Hz, 1H), 7.10 (d, $J = 1.7$ Hz, 1H), 7.04 (s, 1H), 6.94 – 6.87 (m, 1H), 4.16 (s, 2H), 3.89 (d, $J = 7.2$ Hz, 2H), 3.84 (s, 3H), 1.67 (s, 3H), 1.43 (s, 9H).

5.1.6.2. *N*-(1-Cyano-3-methylazetidin-3-yl)-3'-methoxy-[1,1'-biphenyl]-4-carboxamide (compound 49; Table 2).

This compound was prepared according to Method A, steps c-e). ¹H NMR (500 MHz, CDCl₃) δ 7.82 (d, *J* = 8.2 Hz, 2H), 7.66 (d, *J* = 8.2 Hz, 2H), 7.38 (t, *J* = 7.9 Hz, 1H), 7.19 (d, *J* = 7.7 Hz, 1H), 7.13 (s, 1H), 6.94 (dd, *J* = 8.1, 2.0 Hz, 1H), 6.52 (s, 1H), 4.56 (d, *J* = 7.8 Hz, 2H), 4.07 (d, *J* = 7.9 Hz, 2H), 3.87 (s, 3H), 1.73 (s, 3H); MS (ES) *m/z* 322.4641 [M+1]⁺; purity 98%, retention time 4.42 min.

5.1.6.3. *Tert*-butyl 3-((3'-methoxy-[1,1'-biphenyl])-4-sulfonamido)-3-methylazetidine-1-carboxylate (46, *Z* = SO₂; scheme 6).

Step d). To a stirred solution 3'-methoxy-[1,1'-biphenyl]-4-sulfonyl chloride (141 mg, 0.5mmol), and *tert*-butyl 3-amino-3-methylazetidine-1-carboxylate (93 mg, 0.5 mmol) in dichloromethane (20 mL) was added *N,N*-diisopropyl-ethylamine (193 mg, 1.5 mmol). The resulting reaction mixture was stirred at room temperature for 16 hours. After the completion of the reaction (monitored by TLC) the solvent was removed under vacuum. Water was added (10 mL) and the mixture was extracted with ethyl acetate (3x20 mL). The combined extracts were dried over Na₂SO₄ and concentrated under reduced pressure. The residue was purified on silica gel (Biotage; eluting solvents hexane: EtOAc 4/1 ratio) to give *tert*-butyl 3-((3'-methoxy-[1,1'-biphenyl])-4-sulfonamido)-3-methylazetidine-1-carboxylate in as a colorless solid (212 mg, 98% yield); ¹H NMR (500 MHz, CDCl₃) δ 7.92 (d, *J* = 8.5 Hz, 2H), 7.73 (d, *J* = 8.5 Hz, 2H), 7.40 (t, *J* = 8.0 Hz, 1H), 7.19 (d, *J* = 7.7 Hz, 1H), 7.14 – 7.11 (m, 1H), 6.97 (dd, *J* = 8.2, 1.9 Hz, 1H), 4.60 (d, *J* = 8.1 Hz, 2H), 3.92 (d, *J* = 9.6 Hz, 2H), 3.88 (s, 3H), 3.80 (s, 2H), 2.45 (t, *J* = 7.3 Hz, 2H), 1.45 (s, 9H).

The following compound was prepared according to Methods A and F.

5.1.6.4. 3-((3'-Methoxy-[1,1'-biphenyl]-4-yl)sulfonyl)-3-methylazetidine-1-carbonitrile (compound 50; Table 2).

¹H NMR (500 MHz, CDCl₃) δ 7.93 (d, *J* = 8.3 Hz, 2H), 7.74 (d, *J* = 8.4 Hz, 2H), 7.41 (t, *J* = 7.9 Hz, 1H), 7.19 (d, *J* = 7.6 Hz, 1H), 7.13 (s, 1H), 7.01 – 6.95 (m, 1H), 4.92 (s, 1H), 4.31 (d, *J* = 8.1 Hz, 2H), 3.91 (d, *J* = 8.2 Hz, 2H), 3.88 (s, 3H), 1.53 (s, 3H).; MS (ES) *m/z* 358.4389 [M+1]⁺; purity 100%, retention time 4.51 min.

6. Biochemical Pharmacology

6.1. NAAA inhibitor fluorescent assay: Compounds were assessed in a fluorescence-based assay for NAAA inhibition with *N*-(4-methyl coumarin) palmitamide (PAMCA) as the substrate.⁵³ For three-point concentration inhibition assays with hNAAA the following procedure was used. Purified activated hNAAA^{53, 65} (final concentration of 0.25 $\mu\text{g}/\text{mL}$) was incubated in assay buffer (100 mM citrate-phosphate buffer, pH 4.5, 3 mM DTT, 0.1% Triton X-100, 0.05% BSA, and 150 mM NaCl) made up to a total volume of 180 μL , followed by addition of the compound dissolved in 10 μL DMSO (along with DMSO neat for the control sample) with the final concentrations for each compound of 100, 10, and 1 μM , in triplicate on a 96 well plate. These samples were allowed to incubate for 90 min at room temperature and then 10 μL of a PAMCA stock solution in DMSO (final PAMCA concentration [5 μM]) was added. After 5 minutes of agitation on a shaking plate, the reaction was allowed to proceed at 37 °C for 90 minutes, with fluorescence readings taken every 10 minutes at a wavelength of 460 nm (using an excitation wavelength of 360 nm) on a Synergy HT Plate Reader using Gen5 software from Bio-Tek. The enzyme activity was calculated by converting the relative fluorescence units to AMC formed, using a standard curve of AMC. For compounds that inhibited hNAAA in range $\text{IC}_{50} < 1 \mu\text{M}$ full inhibition curves using eight different concentrations of inhibitor (8-point assay) were generated. The assay procedure used was the same as the three-point assay. Inhibition constants were calculated using pro Fit software (Quantum Soft, Uetikon am See, Switzerland) and a Levenberg-Marquardt.

6.2. Determination of NAAA potencies (k_{inact}/K_i values). The potency of cyanamides inhibitors was determined by the second order rate constants k_{inact}/K_i values using an enzyme-coupled NAAA assay in 96-well microplates as described previously⁶⁶. The overall potency, k_{inact}/K_i values, will be calculated from the slope, $k_{\text{inact}}/[K_i (1 + [S]/K_m)]$, which is obtained from the k_{obs} equation as described⁶⁷. NAAA inactivation rates in the absence of inhibitors are subtracted from all k_{obs} values obtained in the presence of inhibitors.

6.3. MGL and FAAH inhibitor fluorescent assay: Human-recombinant FAAH (hFAAH) and MGL (hMGL) were expressed in *E. coli* and purified as described.⁵⁷ A high-throughput fluorometric screening assay for FAAH inhibition using a fluorescent substrate, arachidonoyl 7-amino-4-methylcoumarin amide (AAMCA), was performed as reported.⁵⁶ MGL assays used the

fluorescent substrate arachidonoyl, 7-hydroxy-6-methoxy-4-methylcoumarin ester (AHMMCE).⁵⁷ IC₅₀ values were calculated using Prism software (GraphPad).

6.4 ABHD6 inhibitor fluorescent assay: Compounds were assessed in a high throughput fluorescence-based assay for their ability to inhibit the full-length hABHD6 enzyme. We used the fluorogenic substrate arachidonoyl, 7-hydroxy-6-methoxy-4-methylcoumarin ester (AHMMCE)⁵⁷ that is hydrolyzed to the fluorescent product HMMCE in the presence of active ABHD6 enzyme.

6.5. Cathepsin K assay: Compounds were pre-incubated for 120 min at 37 °C recombinant human Cathepsin K enzyme (Enzo; BML-SE553-0010). We used the fluorogenic substrate Z-Phe-Arg-AMC (Enzo; BML-P139) for the reaction and the enzyme activity was measured from the increase of OD at 405 nm.⁴⁵

6.6. rCB1, hCB2, and mCB2 Binding Assay: Selected compounds were tested for their ability to bind to CB1 and CB2 receptors using rat brain⁵⁹ or HEK293 cell membranes expressing mouse CB2 (mCB2) or human CB2 (hCB2),⁶⁰⁻⁶² respectively, as described via competition-equilibrium binding using [³H]CP-55,940.^{61-63, 68}

6.7. Stability in plasma and buffer: Compound solutions (200 µM) were made in mouse, rat or human plasma, buffer containing 0.1% BSA or artificial gastric juice. After quenching with acetonitrile, the samples were analyzed by HPLC to predict in vivo plasma half-lives.^{69, 70}

6.8. Stability towards rat liver microsomal preparations: Compounds solution (1 µM) were pre-incubated with rat liver microsomal protein (Celsis) at 37°C before the reaction is initiated with NADPH or buffer (control).^{71, 72} Following protein precipitation, the samples will be analyzed using a LC-MS/MS in SRM mode.

7. Computational Studies

7.1. Modeling methods. The computational studies were conducted in Schrodinger Suite (Version 2018-3). The ligands were prepared in the OPLSe3 force field using Ligprep module⁷³. Induced-fit docking (IFD)⁷⁴ and covalent docking⁷⁵ used Glide and conducted with XP (extra

precision) mode in OPLS3e force field^{76, 77}. MM-GBSA rescoring was conducted using Prime module.

7.2. Computational (*in silico*) analysis of physicochemical properties of ligands: *In silico* ligand screening with commercial computational software (Schrodinger Suite 2018-3) used to assess early ADME/pharmacokinetic properties of the proposed compounds in areas as Lipinski rules, ligand efficiency, topological polar surface area (tPSA), cytochrome P450 stability profile, pKa, aqueous solubility, and lipophilicity (ClogP).

8. Supplementary data

Full experimental details for the preparation of all compounds described in Tables 1 and 2, the methods of testing the compounds, and the molecular modeling methods for the design of the new inhibitors have been provided in the supplemental section.

Funding: This work was supported by a NIH grant Molecular Basis, R01-DA003801 (A.M.).

References

1. Pontis S, Ribeiro A, Sasso O and Piomelli D. Macrophage-derived lipid agonists of PPAR- α as intrinsic controllers of inflammation. *Crit Rev Biochem Mol Biol*. 2016; 51: 7-14.
2. Bonezzi FT, Sasso O, Pontis S, et al. An Important Role for N-Acylethanolamine Acid Amidase in the Complete Freund's Adjuvant Rat Model of Arthritis. *The Journal of pharmacology and experimental therapeutics*. 2016; 356: 656-63.
3. Ribeiro A, Pontis S, Mengatto L, et al. A Potent Systemically Active N-Acylethanolamine Acid Amidase Inhibitor that Suppresses Inflammation and Human Macrophage Activation. *ACS chemical biology*. 2015; 10: 1838-46.
4. Bandiera T, Ponzano S and Piomelli D. Advances in the discovery of N-acylethanolamine acid amidase inhibitors. *Pharmacol Res*. 2014; 86: 11-7.
5. Neish AS. Acute inflammation: endogenous cannabinoids mellow the harsh proinflammatory environment. *The Journal of clinical investigation*. 2018; 128: 3750-1.

6. Turcotte C, Chouinard F, Lefebvre JS and Flamand N. Regulation of inflammation by cannabinoids, the endocannabinoids 2-arachidonoyl-glycerol and arachidonoyl-ethanolamide, and their metabolites. *J Leukoc Biol.* 2015; 97: 1049-70.
7. Ranieri R, Laezza C, Bifulco M, Marasco D and Malfitano AM. Cannabinoids and Neuro-Inflammation: Regulation of Brain Immune Response. *Recent patents on CNS drug discovery.* 2016; 10: 178-203.
8. Nagarkatti P, Pandey R, Rieder SA, Hegde VL and Nagarkatti M. Cannabinoids as novel anti-inflammatory drugs. *Future medicinal chemistry.* 2009; 1: 1333-49.
9. Koning GA, Schiffelers RM, Wauben MH, et al. Targeting of angiogenic endothelial cells at sites of inflammation by dexamethasone phosphate-containing RGD peptide liposomes inhibits experimental arthritis. *Arthritis and rheumatism.* 2006; 54: 1198-208.
10. Darmani NA, Izzo AA, Degenhardt B, et al. Involvement of the cannabimimetic compound, N-palmitoyl-ethanolamine, in inflammatory and neuropathic conditions: review of the available pre-clinical data, and first human studies. *Neuropharmacology.* 2005; 48: 1154-63.
11. Costa B, Conti S, Giagnoni G and Colleoni M. Therapeutic effect of the endogenous fatty acid amide, palmitoylethanolamide, in rat acute inflammation: inhibition of nitric oxide and cyclooxygenase systems. *British journal of pharmacology.* 2002; 137: 413-20.
12. Gaetani S, Oveisi F and Piomelli D. Modulation of meal pattern in the rat by the anorexic lipid mediator oleoylethanolamide. *Neuropsychopharmacology : official publication of the American College of Neuropsychopharmacology.* 2003; 28: 1311-6.
13. Okamoto Y, Morishita J, Tsuboi K, Tonai T and Ueda N. Molecular characterization of a phospholipase D generating anandamide and its congeners. *J Biol Chem.* 2004; 279: 5298-305.
14. LoVerme J, La Rana G, Russo R, Calignano A and Piomelli D. The search for the palmitoylethanolamide receptor. *Life sciences.* 2005; 77: 1685-98.
15. Esposito G, Capoccia E, Turco F, et al. Palmitoylethanolamide improves colon inflammation through an enteric glia/toll like receptor 4-dependent PPAR-alpha activation. *Gut.* 2014; 63: 1300-12.
16. Calignano A, La Rana G, Giuffrida A and Piomelli D. Control of pain initiation by endogenous cannabinoids. *Nature.* 1998; 394: 277-81.

17. Jaggar SI, Hasnie FS, Sellaturay S and Rice AS. The anti-hyperalgesic actions of the cannabinoid anandamide and the putative CB2 receptor agonist palmitoylethanolamide in visceral and somatic inflammatory pain. *Pain*. 1998; 76: 189-99.
18. Barrie N and Manolios N. The endocannabinoid system in pain and inflammation: Its relevance to rheumatic disease. *Eur J Rheumatol*. 2017; 4: 210-8.
19. Cravatt BF, Giang DK, Mayfield SP, Boger DL, Lerner RA and Gilula NB. Molecular characterization of an enzyme that degrades neuromodulatory fatty-acid amides. *Nature*. 1996; 384: 83-7.
20. Ueda N, Yamanaka K and Yamamoto S. Purification and characterization of an acid amidase selective for N-palmitoylethanolamine, a putative endogenous anti-inflammatory substance. *The Journal of biological chemistry*. 2001; 276: 35552-7.
21. Tsuboi K, Takezaki N and Ueda N. The N-acylethanolamine-hydrolyzing acid amidase (NAAA). *Chemistry & biodiversity*. 2007; 4: 1914-25.
22. Borer JS and Simon LS. Cardiovascular and gastrointestinal effects of COX-2 inhibitors and NSAIDs: achieving a balance. *Arthritis Res Ther*. 2005; 7 Suppl 4: S14-22.
23. Mamdani M, Rochon PA, Juurlink DN, et al. Observational study of upper gastrointestinal haemorrhage in elderly patients given selective cyclo-oxygenase-2 inhibitors or conventional non-steroidal anti-inflammatory drugs. *BMJ*. 2002; 325: 624.
24. Keppel Hesselink JM, de Boer T and Witkamp RF. Palmitoylethanolamide: A Natural Body-Owned Anti-Inflammatory Agent, Effective and Safe against Influenza and Common Cold. *Int J Inflam*. 2013; 2013: 151028.
25. Zhao LY, Tsuboi K, Okamoto Y, Nagahata S and Ueda N. Proteolytic activation and glycosylation of N-acylethanolamine-hydrolyzing acid amidase, a lysosomal enzyme involved in the endocannabinoid metabolism. *Biochimica et biophysica acta*. 2007; 1771: 1397-405.
26. Mazzari S, Canella R, Petrelli L, Marcolongo G and Leon A. N-(2-hydroxyethyl)hexadecanamide is orally active in reducing edema formation and inflammatory hyperalgesia by down-modulating mast cell activation. *European journal of pharmacology*. 1996; 300: 227-36.
27. D'Agostino G, La Rana G, Russo R, et al. Acute intracerebroventricular administration of palmitoylethanolamide, an endogenous peroxisome proliferator-activated receptor-alpha agonist,

modulates carrageenan-induced paw edema in mice. *The Journal of pharmacology and experimental therapeutics*. 2007; 322: 1137-43.

28. Lambert DM, Vandevorde S, Diependaele G, Govaerts SJ and Robert AR. Anticonvulsant activity of N-palmitoylethanolamide, a putative endocannabinoid, in mice. *Epilepsia*. 2001; 42: 321-7.

29. Solorzano C, Zhu C, Battista N, et al. Selective N-acylethanolamine-hydrolyzing acid amidase inhibition reveals a key role for endogenous palmitoylethanolamide in inflammation. *Proceedings of the National Academy of Sciences of the United States of America*. 2009; 106: 20966-71.

30. Alhouayek M, Bottemanne P, Subramanian KV, et al. N-Acylethanolamine-hydrolyzing acid amidase inhibition increases colon N-palmitoylethanolamine levels and counteracts murine colitis. *FASEB journal : official publication of the Federation of American Societies for Experimental Biology*. 2015; 29: 650-61.

31. Bachur NR, Masek K, Melmon KL and Udenfriend S. Fatty Acid Amides of Ethanolamine in Mammalian Tissues. *The Journal of biological chemistry*. 1965; 240: 1019-24.

32. Peraza MA, Burdick AD, Marin HE, Gonzalez FJ and Peters JM. The toxicology of ligands for peroxisome proliferator-activated receptors (PPAR). *Toxicol Sci*. 2006; 90: 269-95.

33. Klaunig JE, Babich MA, Baetcke KP, et al. PPARalpha agonist-induced rodent tumors: modes of action and human relevance. *Crit Rev Toxicol*. 2003; 33: 655-780.

34. Glass CK and Ogawa S. Combinatorial roles of nuclear receptors in inflammation and immunity. *Nature reviews Immunology*. 2006; 6: 44-55.

35. Straus DS and Glass CK. Anti-inflammatory actions of PPAR ligands: new insights on cellular and molecular mechanisms. *Trends in immunology*. 2007; 28: 551-8.

36. Tuo W, Leleu-Chavain N, Spencer J, Sansook S, Millet R and Chavatte P. Therapeutic Potential of Fatty Acid Amide Hydrolase, Monoacylglycerol Lipase, and N-Acylethanolamine Acid Amidase Inhibitors. *Journal of medicinal chemistry*. 2017; 60: 4-46.

37. Li Y, Zhou P, Chen H, et al. Inflammation-restricted anti-inflammatory activities of a N-acylethanolamine acid amidase (NAAA) inhibitor F215. *Pharmacol Res*. 2018; 132: 7-14.

38. Li Y, Chen Q, Yang L, et al. Identification of highly potent N-acylethanolamine acid amidase (NAAA) inhibitors: Optimization of the terminal phenyl moiety of oxazolidone derivatives. *European journal of medicinal chemistry*. 2017; 139: 214-21.

39. Duranti A, Tontini A, Antonietti F, et al. N-(2-oxo-3-oxetanyl)carbamic acid esters as N-acylethanolamine acid amidase inhibitors: synthesis and structure-activity and structure-property relationships. *Journal of medicinal chemistry*. 2012; 55: 4824-36.
40. Vitale R, Ottonello G, Petracca R, et al. Synthesis, structure-activity, and structure-stability relationships of 2-substituted-N-(4-oxo-3-oxetanyl) N-acylethanolamine acid amidase (NAAA) inhibitors. *ChemMedChem*. 2014; 9: 323-36.
41. Migliore MD, Pontis SD, Fuentes de Arriba AL, et al. Second-Generation Non-Covalent NAAA Inhibitors are Protective in a Model of Multiple Sclerosis. *Angew Chem Int Ed Engl*. 2016; 55: 11193-7.
42. Solorzano C, Antonietti F, Duranti A, et al. Synthesis and structure-activity relationships of N-(2-oxo-3-oxetanyl)amides as N-acylethanolamine-hydrolyzing acid amidase inhibitors. *Journal of medicinal chemistry*. 2010; 53: 5770-81.
43. Sasso O, Moreno-Sanz G, Martucci C, et al. Antinociceptive effects of the N-acylethanolamine acid amidase inhibitor ARN077 in rodent pain models. *Pain*. 2013; 154: 350-60.
44. Petracca R, Ponzano S, Bertozzi SM, et al. Progress in the development of beta-lactams as N-Acylethanolamine Acid Amidase (NAAA) inhibitors: Synthesis and SAR study of new, potent N-O-substituted derivatives. *European journal of medicinal chemistry*. 2017; 126: 561-75.
45. Falguyret JP, Oballa RM, Okamoto O, et al. Novel, nonpeptidic cyanamides as potent and reversible inhibitors of human cathepsins K and L. *Journal of medicinal chemistry*. 2001; 44: 94-104.
46. Lodola A, Branduardi D, De Vivo M, et al. A catalytic mechanism for cysteine N-terminal nucleophile hydrolases, as revealed by free energy simulations. *PLoS One*. 2012; 7: e32397.
47. Fidelix TS, Soares BG and Trevisani VF. Diacerein for osteoarthritis. *Cochrane Database Syst Rev*. 2006: CD005117.
48. Petrosino S, Ahmad A, Marcolongo G, et al. Diacerein is a potent and selective inhibitor of palmitoylethanolamide inactivation with analgesic activity in a rat model of acute inflammatory pain. *Pharmacol Res*. 2015; 91: 9-14.
49. Zhou P, Xiang L, Yang Y, et al. N-Acylethanolamine acid amidase (NAAA) inhibitor F215 as a novel therapeutic agent for osteoarthritis. *Pharmacol Res*. 2019; 145: 104264.

50. Gorelik A, Gebai A, Illes K, Piomelli D and Nagar B. Molecular mechanism of activation of the immunoregulatory amidase NAAA. *Proceedings of the National Academy of Sciences of the United States of America*. 2018; 115: E10032-E40.
51. Kalgutkar AS and Dalvie DK. Drug discovery for a new generation of covalent drugs. *Expert Opin Drug Discov*. 2012; 7: 561-81.
52. Nakayama S, Atsumi R, Takakusa H, et al. A zone classification system for risk assessment of idiosyncratic drug toxicity using daily dose and covalent binding. *Drug metabolism and disposition: the biological fate of chemicals*. 2009; 37: 1970-7.
53. West JM, Zvonok N, Whitten KM, Vadivel SK, Bowman AL and Makriyannis A. Biochemical and mass spectrometric characterization of human N-acylethanolamine-hydrolyzing acid amidase inhibition. *PloS one*. 2012; 7: e43877.
54. Alapafuja SO, Nikas SP, Bharathan IT, et al. Sulfonyl fluoride inhibitors of fatty acid amide hydrolase. *Journal of medicinal chemistry*. 2012; 55: 10074-89.
55. Patricelli MP, Lashuel HA, Giang DK, Kelly JW and Cravatt BF. Comparative characterization of a wild type and transmembrane domain-deleted fatty acid amide hydrolase: identification of the transmembrane domain as a site for oligomerization. *Biochemistry*. 1998; 37: 15177-87.
56. Ramarao MK, Murphy EA, Shen MW, et al. A fluorescence-based assay for fatty acid amide hydrolase compatible with high-throughput screening. *Analytical biochemistry*. 2005; 343: 143-51.
57. Zvonok N, Pandarinathan L, Williams J, et al. Covalent inhibitors of human monoacylglycerol lipase: ligand-assisted characterization of the catalytic site by mass spectrometry and mutational analysis. *Chemistry & biology*. 2008; 15: 854-62.
58. Shields CM, Zvonok N, Zvonok A and Makriyannis A. Biochemical and Proteomic Characterization of Recombinant Human alpha/beta Hydrolase Domain 6. *Scientific reports*. 2019; 9: 890.
59. Abadji V, Lucas-Lenard JM, Chin C and Kendall DA. Involvement of the carboxyl terminus of the third intracellular loop of the cannabinoid CB1 receptor in constitutive activation of Gs. *J Neurochem*. 1999; 72: 2032-8.

60. Dodd PR, Hardy JA, Oakley AE, Edwardson JA, Perry EK and Delaunoy JP. A rapid method for preparing synaptosomes: comparison, with alternative procedures. *Brain Res.* 1981; 226: 107-18.
61. Guo Y, Abadji V, Morse KL, Fournier DJ, Li X and Makriyannis A. (-)-11-Hydroxy-7'-isothiocyanato-1',1'-dimethylheptyl-delta 8-THC: a novel, high-affinity irreversible probe for the cannabinoid receptor in the brain. *J Med Chem.* 1994; 37: 3867-70.
62. Morse KL, Fournier DJ, Li X, Grzybowska J and Makriyannis A. A novel electrophilic high affinity irreversible probe for the cannabinoid receptor. *Life Sci.* 1995; 56: 1957-62.
63. Lan R, Liu Q, Fan P, et al. Structure-activity relationships of pyrazole derivatives as cannabinoid receptor antagonists. *J Med Chem.* 1999; 42: 769-76.
64. Wu K XY, Zhou P, Qiu Y, Li Y. A New Use for an Old Drug: Carmofur Attenuates Lipopolysaccharide (LPS)-Induced Acute Lung Injury via Inhibition of FAAH and NAAA Activities. *Frontiers in Pharmacology.* 2019; 10.
65. West JM, Zvonok N, Whitten KM, Wood JT and Makriyannis A. Mass spectrometric characterization of human N-acylethanolamine-hydrolyzing acid amidase. *Journal of proteome research.* 2012; 11: 972-81.
66. Mileni M, Johnson DS, Wang Z, et al. Structure-guided inhibitor design for human FAAH by interspecies active site conversion. *Proceedings of the National Academy of Sciences of the United States of America.* 2008; 105: 12820-4.
67. Ahn K, Johnson DS, Mileni M, et al. Discovery and characterization of a highly selective FAAH inhibitor that reduces inflammatory pain. *Chemistry & biology.* 2009; 16: 411-20.
68. Cheng Y and Prusoff WH. Relationship between the inhibition constant (K₁) and the concentration of inhibitor which causes 50 per cent inhibition (I₅₀) of an enzymatic reaction. *Biochem Pharmacol.* 1973; 22: 3099-108.
69. Hale JT, Bigelow JC, Mathews LA and McCormack JJ. Analytical and pharmacokinetic studies with 5-chloro-2'-deoxycytidine. *Biochem Pharmacol.* 2002; 64: 1493-502.
70. Wood JT, Smith DM, Janero DR, Zvonok AM and Makriyannis A. Therapeutic modulation of cannabinoid lipid signaling: metabolic profiling of a novel antinociceptive cannabinoid-2 receptor agonist. *Life Sci.* 2013; 92: 482-91.

71. Mohutsky MA, Chien JY, Ring BJ and Wrighton SA. Predictions of the in vivo clearance of drugs from rate of loss using human liver microsomes for phase I and phase II biotransformations. *Pharmaceutical Research*. 2006; 23: 654-62.
72. Obach RS. Prediction of human clearance of twenty-nine drugs from hepatic microsomal intrinsic clearance data: An examination of in vitro half-life approach and nonspecific binding to microsomes. *Drug Metabolism and Disposition*. 1999; 27: 1350-9.
73. LigPrep, Schrödinger, LLC, New York, NY, 2017.
74. Sherman W, Day T, Jacobson MP, Friesner RA and Farid R. Novel procedure for modeling ligand/receptor induced fit effects. *Journal of medicinal chemistry*. 2006; 49: 534-53.
75. Zhu K, Borrelli KW, Greenwood JR, et al. Docking covalent inhibitors: a parameter free approach to pose prediction and scoring. *Journal of chemical information and modeling*. 2014; 54: 1932-40.
76. Harder E, Damm W, Maple J, et al. OPLS3: A Force Field Providing Broad Coverage of Drug-like Small Molecules and Proteins. *J Chem Theory Comput*. 2016; 12: 281-96.
77. Friesner RA, Murphy RB, Repasky MP, et al. Extra precision glide: docking and scoring incorporating a model of hydrophobic enclosure for protein-ligand complexes. *Journal of medicinal chemistry*. 2006; 49: 6177-96.

Fig. 1 Known NAAA inhibitors

Fig. 2 Design of cyanamides hNAAA inhibitors

Fig. 3 Ligand interaction diagram of the lowest binding energy pose of **17f** (Table 1) within the hNAAA binding pocket. The hydrogen bonds are represented by beige lines. The proximal phenyl group is forming π -stacking interactions with Tyr177 and Tyr146 represented by green lines.

Fig. 4 Covalent docking of **17f** (Table 1) with hNAAA crystal structure with the leaving group no longer attached. A Connolly surface shown as electrostatic potential (red-white-blue) was used to represent the shape of the binding pocket. Only the key residues (green) and the ligand (white) are shown. All other atoms are colored by atom type. The ligand orients into the binding pocket making several π -stacking interactions shown in blue dashed lines. Hydrogen bonds are indicated by yellow dashed lines.

Fig. 5 Induced-fit docking of **17f** (Table 1) with hNAAA crystal structure. A Connolly surface shown as electrostatic potential (red-white-blue) was used to represent the shape of the binding pocket. Only the key residues (green) and the ligand (white) are shown. All other atoms are colored by atom type. The ligand orients into the binding pocket making several π -stacking interactions shown in blue dashed lines. Hydrogen bonds are indicated by yellow dashed lines

Fig. 6 Induced-fit docking of **30f** (Table 2) with hNAAA crystal structure. A Connolly surface shown as electrostatic potential (red-white-blue) was used to represent the shape of the binding pocket. Only the key residues (green) and the ligand (white) are shown. All other atoms are colored by atom type. The ligand orients into the binding pocket making several π -stacking interactions shown in blue dashed lines. Hydrogen bonds are indicated by yellow dashed lines.

Figure 1

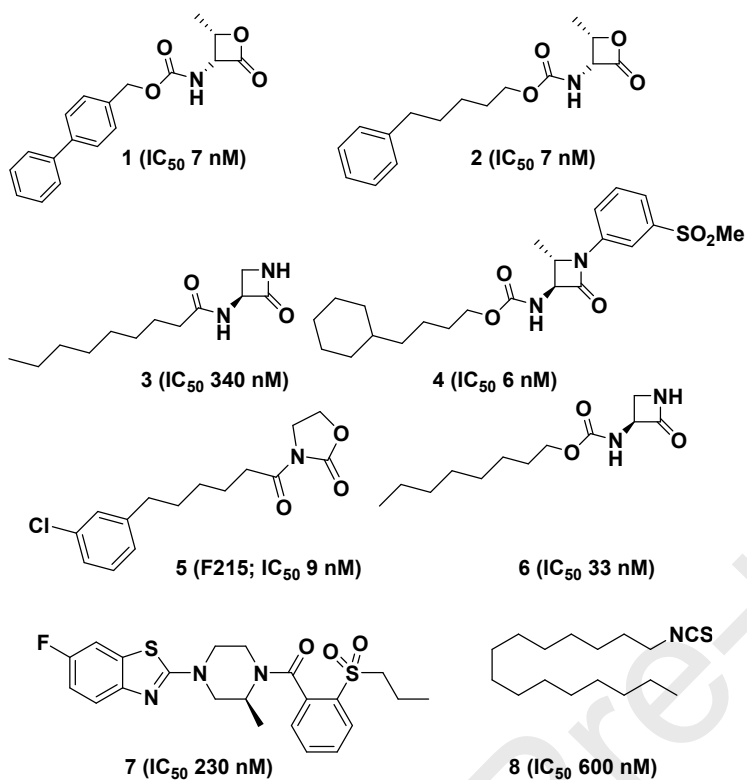


Figure 2

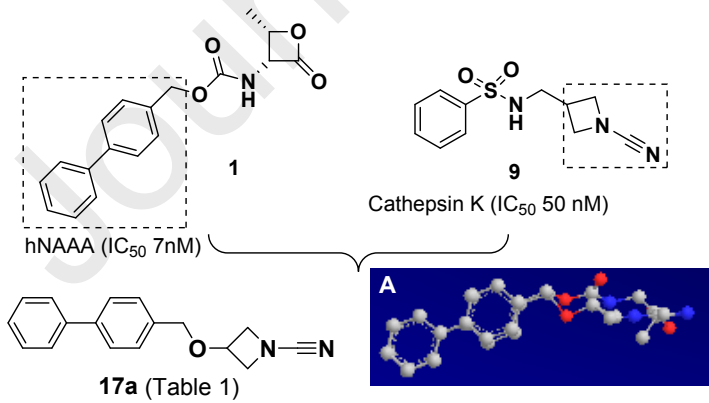


Figure 3

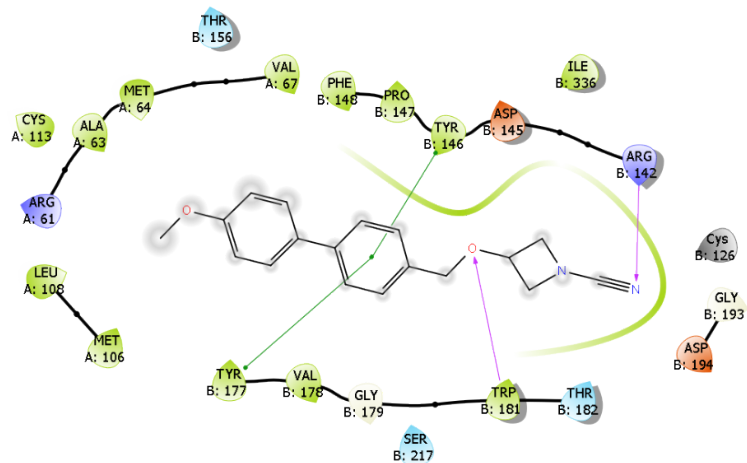


Figure 4

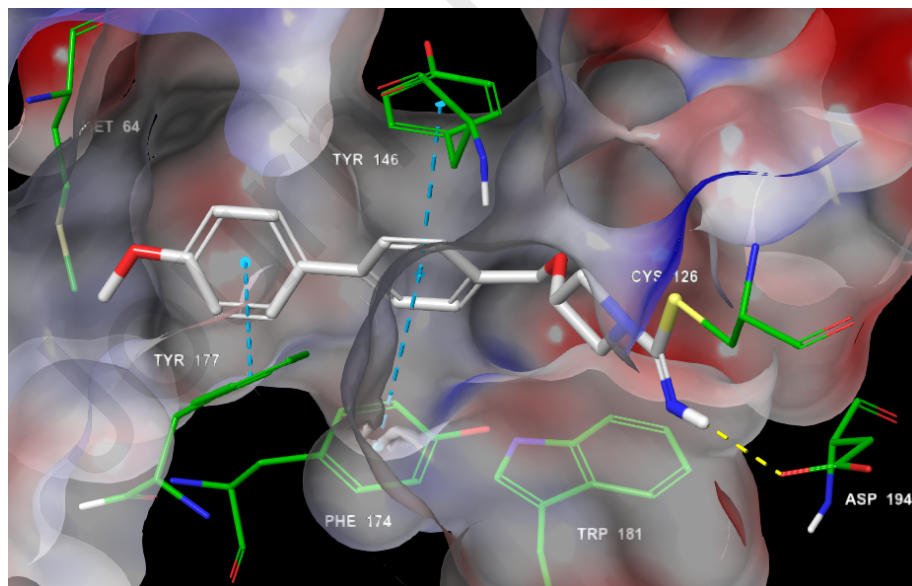


Figure 5

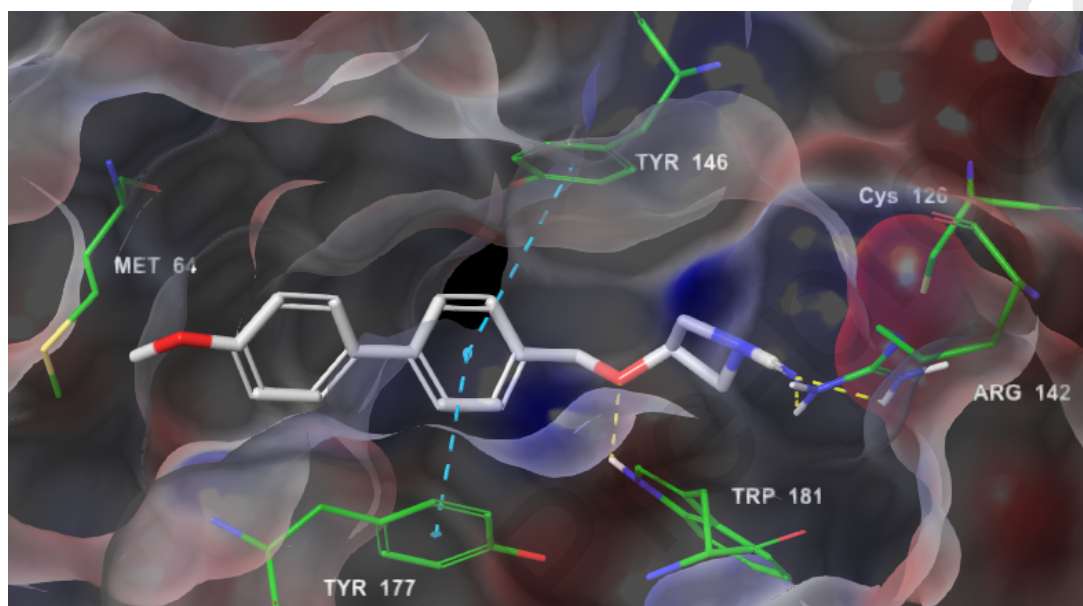
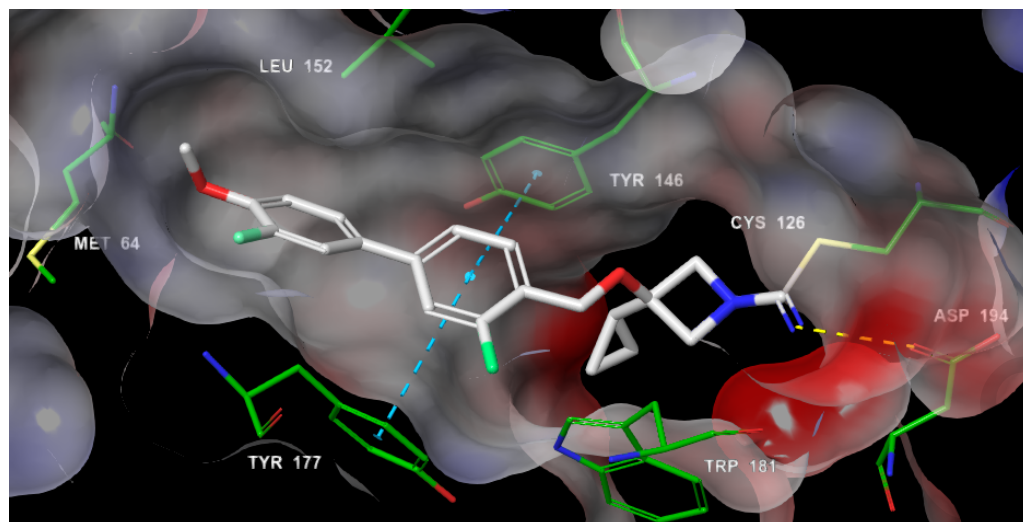


Figure 6



We wish to confirm that there are no known conflicts of interest associated with this publication and there has been no significant financial support for this work that could have influenced its outcome.

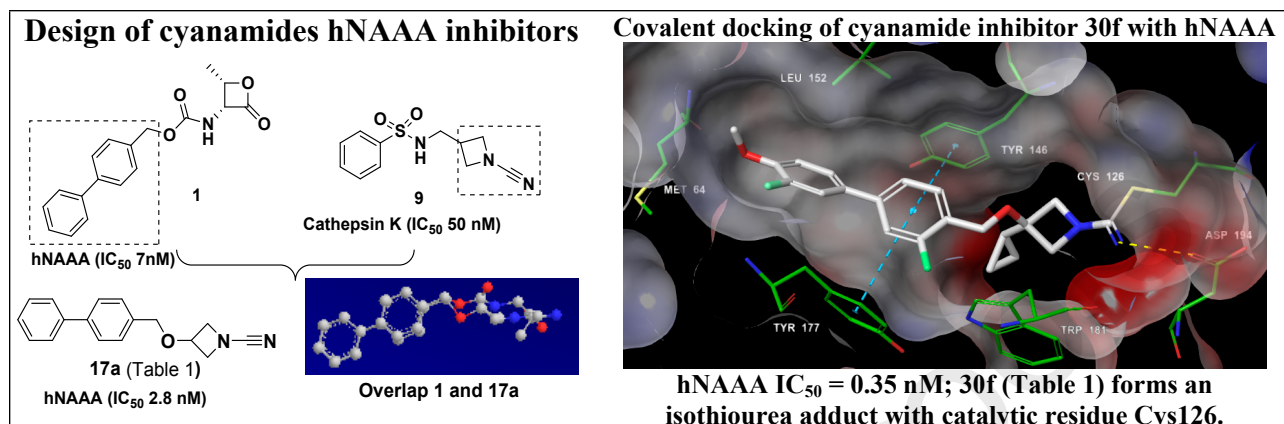
We confirm that the manuscript has been read and approved by all named authors and that there are no other persons who satisfied the criteria for authorship but are not listed. We further confirm that the order of authors listed in the manuscript has been approved by all of us.

We confirm that we have given due consideration to the protection of intellectual property associated with this work and that there are no impediments to publication, including the timing of publication, with respect to intellectual property. In so doing we confirm that we have followed the regulations of our institutions concerning intellectual property.

We further confirm that any aspect of the work covered in this manuscript that has involved either experimental animals or human patients has been conducted with the ethical approval of all relevant bodies and that such approvals are acknowledged within the manuscript. We understand that the Corresponding Author is the sole contact for the Editorial process (including Editorial Manager and direct communications with the office). He/she is responsible for communicating with the other authors about progress, submissions of revisions and final approval of proofs. We confirm that we have provided a current, correct email address which is accessible by the Corresponding Author and which has been configured to accept email from (m.malamas@northeastern.edu)

Michael Malamas, PhD.

Graphical Abstract



Scheme 1

Reagents: (a) NaBH₄, MeOH, THF; (b) 4-bromobenzyl bromide, NaH, DMF; (c) trifluoroacetic acid, CH₂Cl₂; (d) R₁-B(OH)₂, K₂CO₃, Pd(PPh₃)₄, dioxane, H₂O; (e) CNBr, Et₃N, CH₂Cl₂; (f) MeSO₂Cl, Et₃N, CH₂Cl₂; (g) Ph-Ph-OH, NaH, DMF

Scheme 2

Reagents: (a) phenol, K₂CO₃, DMF; (b) NaBH₄, MeOH; (c) PBr₃, THF; (d) NaH, DMF; (e) TFA, CH₂Cl₂; (f) CNBr, Et₃N, CH₂Cl₂; (g) R₂-B(OH)₂, CsF, Pd(PPh₃)₄, dimethoxyethane

Scheme 3

Reagents: (a) R₃MgBr or R₃-Li, THF; (b) 4N NaOH, Bu₄NBr, 4-Br-benzyl bromide, CH₂Cl₂; (c) R₁-B(OH)₂, K₂CO₃, Pd(PPh₃)₄, dioxane, H₂O; (d) TFA, CH₂Cl₂; (e) CNBr, Et₃N, CH₂Cl₂; (f) R₁-B(OH)₂, CsF, Pd(PPh₃)₄, dimethoxyethane

Scheme 4

Reagents: (a) TsOH, CH₂Cl₂; (b) CH₃CH(Cl)OCOC₂H₅, CH₂Cl₂; (c) CNBr, Et₃N, CH₂Cl₂; (d) R₁-B(OH)₂, CsF, Pd(PPh₃)₄, dimethoxyethane

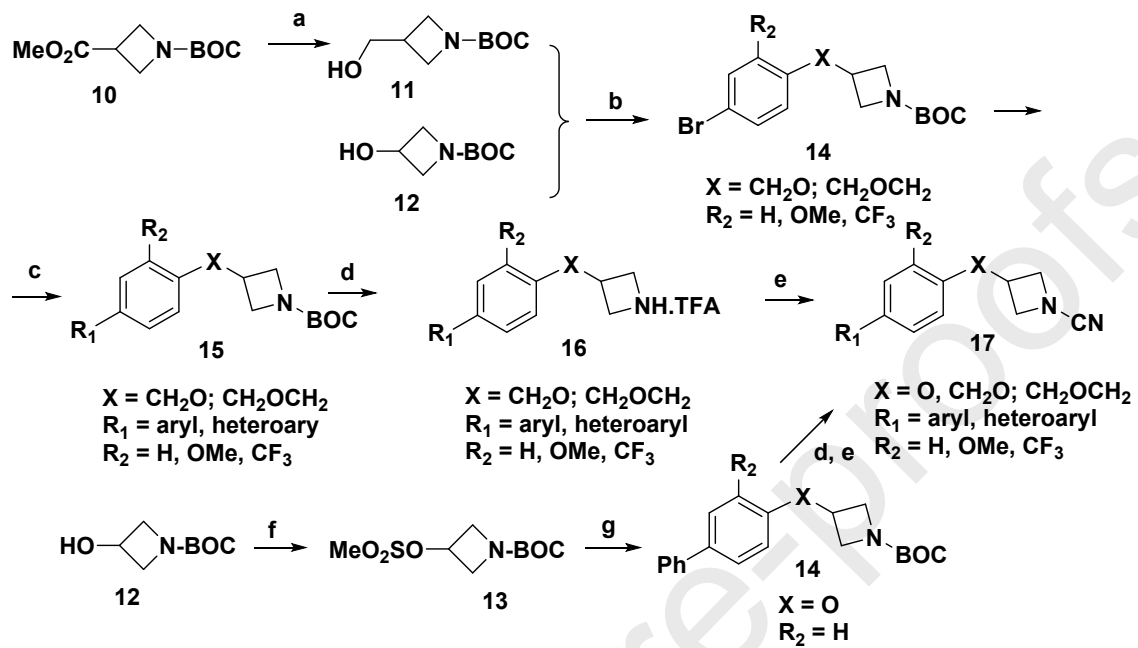
Scheme 5

Reagents: (a) Na(OAc)₃BH, AcOH, THF; (b) 3-F, 4-OMePhB(OH)₂, K₂CO₃, Pd(PPh₃)₄, dioxane, H₂O; (c) TFA, CH₂Cl₂; (d) CNBr, Et₃N, CH₂Cl₂

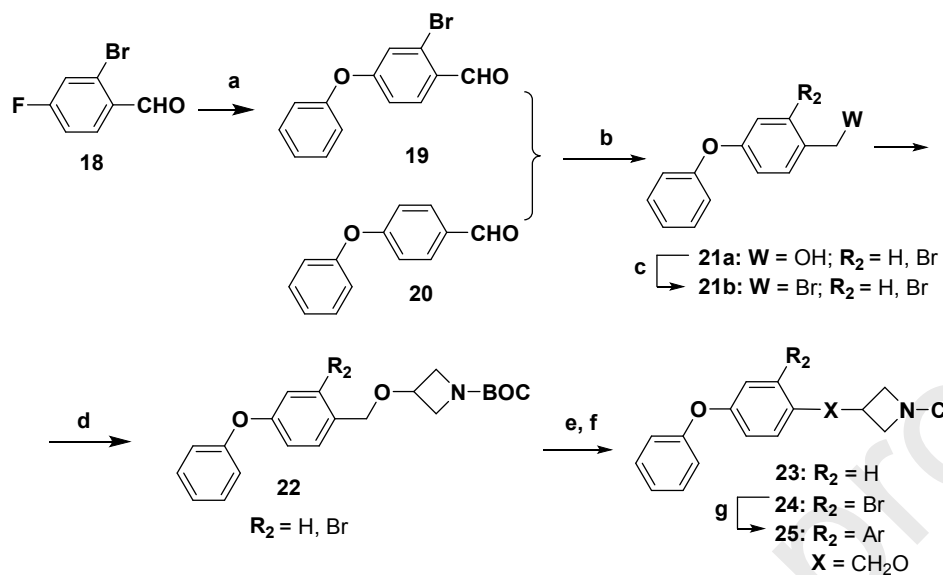
Scheme 6

Reagents: (a) HBTU, (i-Pr)₂EtN, DMF; (b) TFA, CH₂Cl₂; (c) CNBr, Et₃N, CH₂Cl₂; (d) (i-Pr)₂EtN, CH₂Cl₂

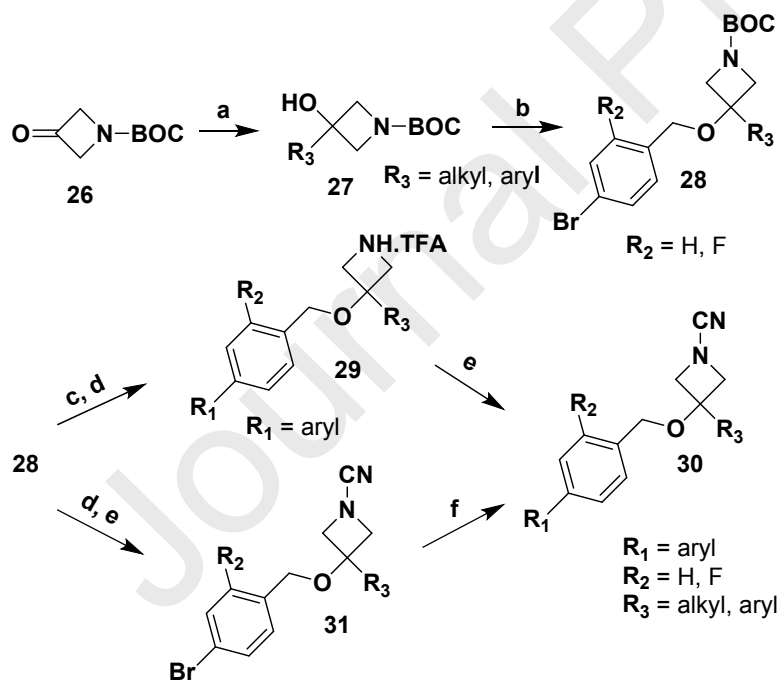
Scheme 1



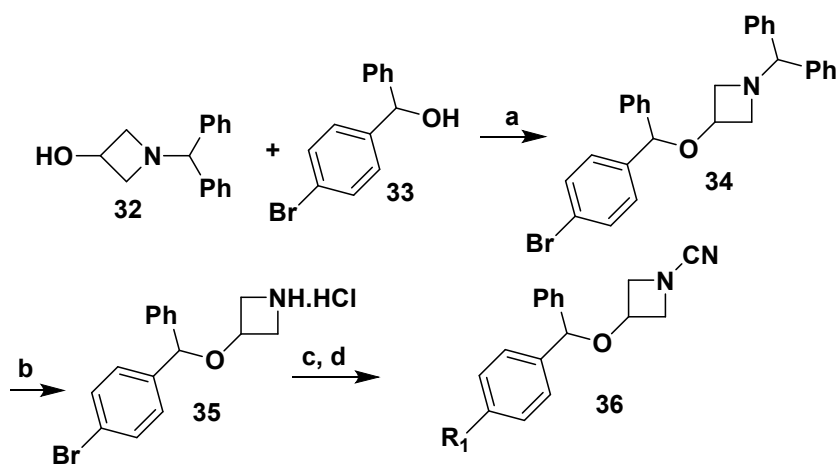
Scheme 2



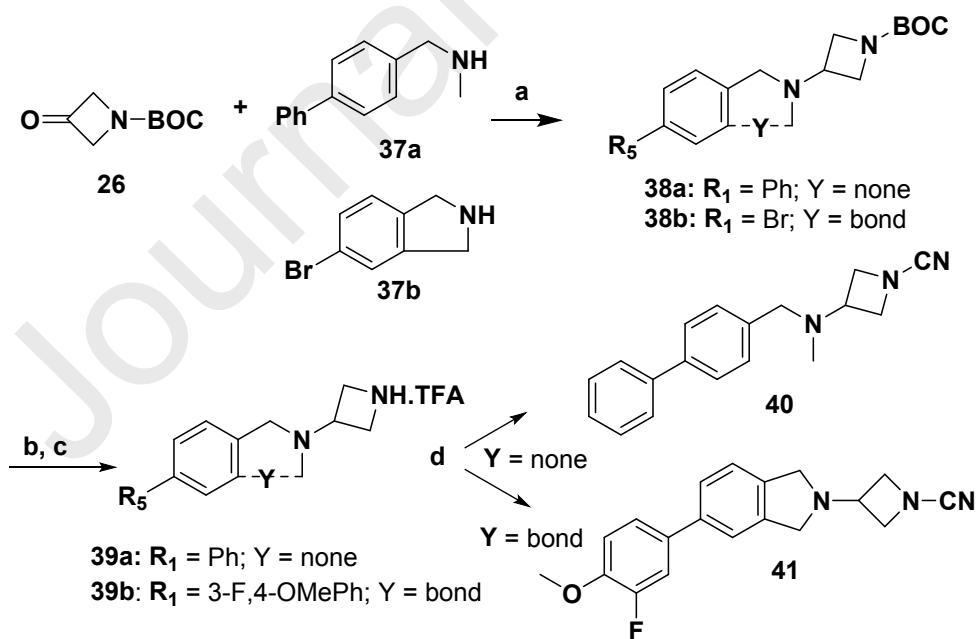
Scheme 3



Scheme 4



Scheme 5



Scheme 6

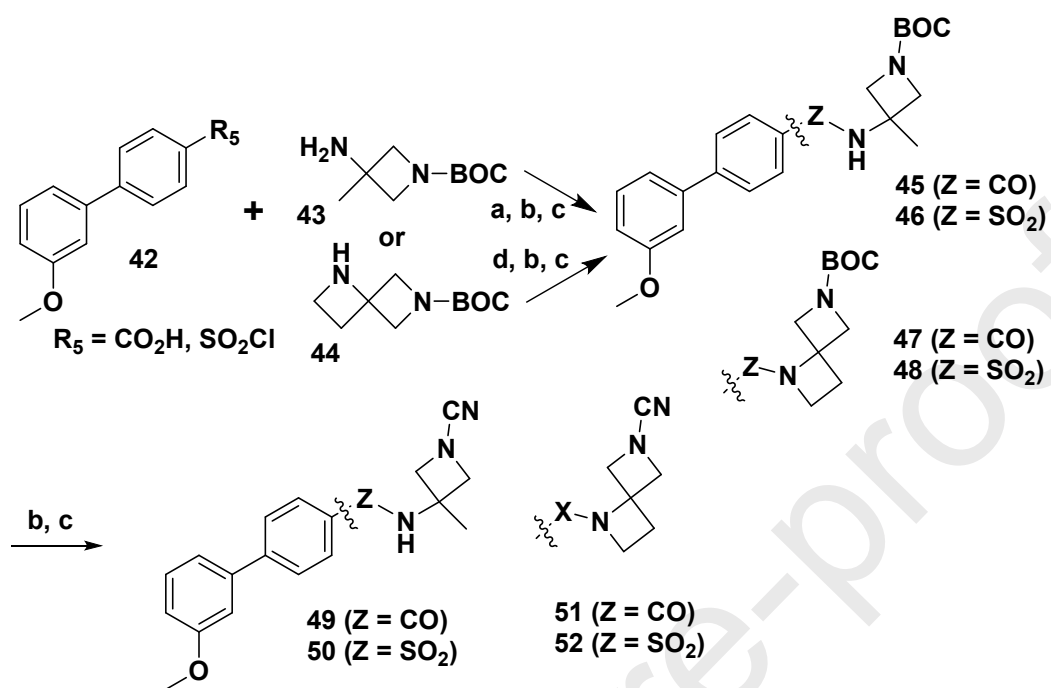
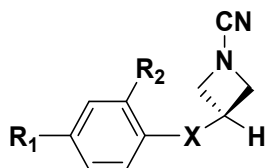
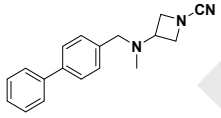
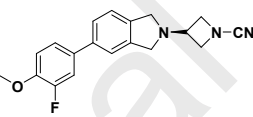
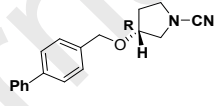
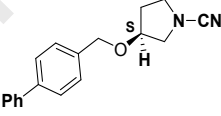
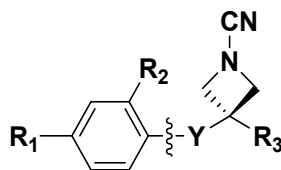


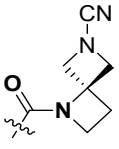
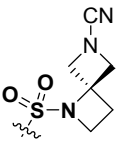
Table 1. Mono-substituted cyanamides hNAAA inhibitors

Compd	R ₁	R ₂	X	hNAAA	
				IC ₅₀ (nM) ± SD ^a	K _{inact} /K _I M ⁻¹ s ⁻¹
Biphenyl analogs					
17a	Ph	H	CH ₂ O	2.8±0.3	3.03x10 ⁶
17b	Ph	H	O	29±2	-
17c	Ph	H	CH ₂ OCH ₂	3.4±0.5	3.04 x10 ⁶
17d	3-OMePh	H	CH ₂ O	0.89±0.19	3.05 x10 ⁶
17e	3-benzyloxyPh	H	CH ₂ O	1.4	-
17f	4-OMePh	H	CH ₂ O	0.94±0.06	3.25 x10 ⁶
17g	2,3-di-OMePh	H	CH ₂ O	0.88±0.26	8.40 x10 ⁶
17h	2,6-di-OMePh	H	CH ₂ O	67.5	-
17i	4-Me-Ph	H	CH ₂ O	0.46±0.26	2.24 x10 ⁶
17j	4-CF ₃ -Ph	H	CH ₂ O	1.6±0.2	2.74 x10 ⁶
17k	4-F-Ph	H	CH ₂ O	0.68±0.25	2.09 x10 ⁶
17l	4-OMe- <i>m</i> -pyridyl	H	CH ₂ O	40±4	-
17m	2-OMe- <i>m</i> -pyridyl	H	CH ₂ O	5.8±0.4	-
17n	<i>m</i> -pyridyl	H	CH ₂ O	12±5	-
17o	3-OMePh	F	CH ₂ O	0.47±0.17	1.73 x10 ⁶
17p	3-OMePh	CF ₃	CH ₂ O	0.85±0.21	1.40 x10 ⁶
17q	3-OMePh	OMe	CH ₂ O	2.8±0.2	-
Benzyloxy analogs					
23	PhO	H	CH ₂ O	1.1±0.05	1.33 x10 ⁶

24	PhO	Br	CH ₂ O	1.03±0.05	-
25a	PhO	Ph	CH ₂ O	8.5±1	-
25b	PhO	2-OMe-Ph	CH ₂ O	23.7±2.2	-
25c	PhO	4-OMe-Ph	CH ₂ O	5.7±0.3	-
25d	PhO	4-CN-Ph	CH ₂ O	2.5±0.3	-
25e	PhO	2-CN-Ph	CH ₂ O	6.6±0.3	-
Benzhydryl-type analogs					
36a	3-OMePh	H	CH(Ph)O	11.6±0.5	-
36b	3,5-isoxazole	H	CH(Ph)O	91.2±5.7	-
36c	N-Me-pyrazole	H	CH(Ph)O	74.7±7.81	-
Nitrogen-linked analogs					
40				20.8	-
41				1.6±0.2	-
Pyrrolidine cyanamides					
42				26.4±1.1	-
43				315±17.6	-

^a IC₅₀s performed in triplicate and determined from eight concentrations in the hNAAA inhibition assay. Activity measured after 90 min pre-incubation of the inhibitor and enzyme prior to the addition of the fluorogenic substrate N-(4-methyl coumarin) palmitamide (PAMCA). IC₅₀ values were calculated using Prism software (GraphPad).

Table 2. Di-substituted cyanamides hNAAA inhibitors

Compd	R ₁	R ₂	R ₃	Y	IC ₅₀ (nM) ± SD ^a or % inhibition @ 1 uM		
					hNAAA	hFAAH	hMGL
3,3-Di-substituted azetidines							
30a	3-OMePh	H	Me	CH ₂ O	1.8±0.3	0.36±0.02	1058±47
30b	3-OMePh	H	Ph	CH ₂ O	9.1±0.6	61±4	19.5%
30c	benzo[d][1,3]dioxole	H	Ph	CH ₂ O	9.2±0.9	99%	59%
30d	2,3-dihydrobenzo[b][1,4]dioxine	H	Ph	CH ₂ O	6.1±0.8	99%	13.5%
30e	4-OMe,3F-Ph	F	<i>m</i> -pyridyl	CH ₂ O	4.6±0.4	2.0±0.2	66%
30f	4-OMe,3F-Ph	F	cyclopropane	CH ₂ O	0.35±0.03	1.0±0.3	472±87
49	3-OMePh	H	Me	CONH	1.58±0.08	23%	11%
50	3-OMePh	H	Me	SO ₂ NH	3.2±0.2	17.8±2.2	19%
3,3-Spiro-azetidines							
51	3-OMePh	H			6.5±0.4	6%	4%
52	3-OMePh	H			2.8±0.1	10.2±1.9	14%

^a IC₅₀s performed in triplicate and determined from eight concentrations in the hNAAA inhibition assay. Activity measured after 90 min pre-incubation of the inhibitor and enzyme prior to the addition of the fluorogenic substrate N-(4-methyl coumarin) palmitamide (PAMCA). IC₅₀ values were calculated using Prism software (GraphPad).

Table 3. Plasma and gastric fluids stability of cyanamides hNAAA inhibitors

Compd	Plasma stability $t_{1/2}$ min		Gastric fluids stability $t_{1/2}$ min
	Human	Rat	
17d	204	189	450
17o	228	184	271
30f	127	-	-
49	902	-	-
50	221	-	-
51	458	-	-
52	180	-	-

Table 4. Microsomal stability of cyanamides hNAAA inhibitors

Compd	Microsomal stability $t_{1/2}$ min	
	Human	Rat
17d	11.2	10
17j	6.8	8.9
17o	5.7	7.9
30b	15.3	14.5
40	11.3	-
41	14.7	4.4